Astronomy & Astrophysics manuscript no. aa10475v1
September 5, 2008
© ESO 2008

arXiv:0809.0990v1 [astro-ph] 5 Sep 2008

New deep *XMM-Newton* observations to the west of the σ Orionis cluster

J. López-Santiago and J. A. Caballero

Departamento de Astrofísica y Ciencias de la Atmósfera, Facultad de Ciencias Físicas, Universidad Complutense de Madrid, E-28040 Madrid, Spain

Received 27 June 2008 / Accepted 02 September 2008

ABSTRACT

Aims. The objective of this study is to determine the general X-ray properties of the young stars in the external regions of the σ Orionis cluster ($\tau \sim 3$ Ma, $d \sim 385$ pc) and yield constraints on the X-ray emission of brown dwarfs.
Methods. We carried out a careful analysis of public data taken in an unexplored region to the west of the centre of the cluster with the three EPIC cameras onboard the *XMM-Newton* mission. We looked for new X-ray young stars among the 41 identified X-ray sources in the area with maximum likelihood parameters $L > 15$ by cross-correlation with the USNO-B1, DENIS, and 2MASS databases.
Results. Based on colour-colour, colour-magnitude, and hardness ratio diagrams, and previous spectroscopic, astrometric, and infrared-flux excess information, we classified the optical/near-infrared counterparts of the X-ray sources into: young stars (15), field stars (4), galaxies (19), and sources of unknown nature (3). Most of the X-ray detections, including those of nine young stars, are new. We derived the X-ray properties (e.g. temperatures, metallicities, column densities) of the twelve young stars with the largest signal-to-noise ratios. The X-ray parameters determined here are in well agreement with those found in the cluster centre, where the stellar density is higher. There is no relation between infrared excess and column density from X-ray measurement in our data. We detected flaring events in two young stars of the sample. One of them showed a very large (~ 30) relative increase in flux. Both stars showed high coronal temperatures during the observation. Finally, we determined upper limits to the flux of the young stars and bright brown dwarfs not detected by our searching algorithm.

Key words. open clusters and associations: individual: σ Orionis – stars: activity – X-ray: stars

1. Introduction

The σ Orionis cluster ($\tau \sim 3$ Ma, $d \sim 385$ pc) is a "well-equipped laboratory" for studying the formation, evolution, and astrophysical properties of high-mass, solar-like, and low-mass stars, brown dwarfs, and planetary-mass objects below the deuterium burning mass limit (Walborn 1974; Groote & Hunger 1982; Zapatero et al. 2000; Béjar et al. 2001; Kenyon et al. 2005; Caballero et al. 2007). The cluster takes the name from the Trapezium-like system σ Ori in its centre (we use the abridged name, σ Ori, for the –at least– sextuple system, and the full name, σ Orionis, for the eponymous cluster). In spite of its early discovery (Garrison 1967), it was not until the pioneer works by Wolk (1996) and Walter et al. (1997), who detected an over-density of X-ray emitters and pre-main sequence stars (see Fig. 1), when the σ Orionis cluster started taking importance. Afterwards, the detection of Herbig-Haro objects (Reipurth et al. 1998), brown dwarfs (Béjar et al. 1999), the least massive object directly detected out of the Solar System (S Ori 70; Zapatero Osorio et al. 2002b), and planetary-mass objects with discs (Zapatero Osorio et al. 2007) have transformed σ Orionis in a cornerstone for the study of stellar and substellar populations in very young open clusters. See Caballero (2007a, 2008c) for comprehensive σ Orionis data compilations.

Regarding high energies in the cluster, the soft X-ray emission (0.2–3.5 keV) of σ Ori AF–B (O9.5V + B0.0V + B0.5V – Caballero 2008b; D. M. Peterson et al. in prep.) was first revealed by the *Einstein Observatory* (Chlebowski et al. 1989). The X-ray emission in such an early-type star is thought to come from shock-heated gas in the radiatively driven stellar winds. Berghöfer & Schmitt (1994) found no X-ray variability during a long-term monitoring with the *Röntgensatellit* (*ROSAT*) of the triple system (unresolved in their observations), which showed the stability of their winds. Later, Sanz-Forcada et al. (2004) and Waldron & Cassinelli (2007) presented high energy resolution spectra of σ Ori AF–B obtained with the *X-ray Multi-Mirror Mission - Newton* (*XMM-Newton*) and the *Chandra X-ray Observatory*, respectively. Very recently, Skinner et al. (2008), from data obtained with the High Energy Transmission Grating Spectrometer onboard *Chandra*, considered possible alternatives to the radiative wind shock, including magnetically-confined and colliding wind shocks.

Sanz-Forcada et al. (2004) reported a strong X-ray flare on the magnetic B2Vp star σ Ori E, the second brightest star in the cluster, confirming the previous discovery of a flare on the star by Groote & Schmitt (2004) with *ROSAT* data. Caballero et al. (in prep.) have also detected another flare using alternative *ROSAT* data. However, X-ray flares are not expected in the wind scenario of early-type stars. The low-mass companion hypothesis supported by Sanz-Forcada et al. (2004) and discussed in the literature since the early 1970s (see Landstreet & Borra 1978) has been lately confirmed by Bouy et al. (2008) using a multi-conjugate adaptive optics system (σ Ori E and its fainter companion are separated by only 0.330 arcsec).

In contrast to early-type stars, the origin of the X-ray emission in low-mass stars resides on the high temperatures of their coronae. The first detailed analysis of young, low-mass X-ray

Send offprint requests to: Javier López-Santiago, e-mail: jls@astrax.fis.ucm.es

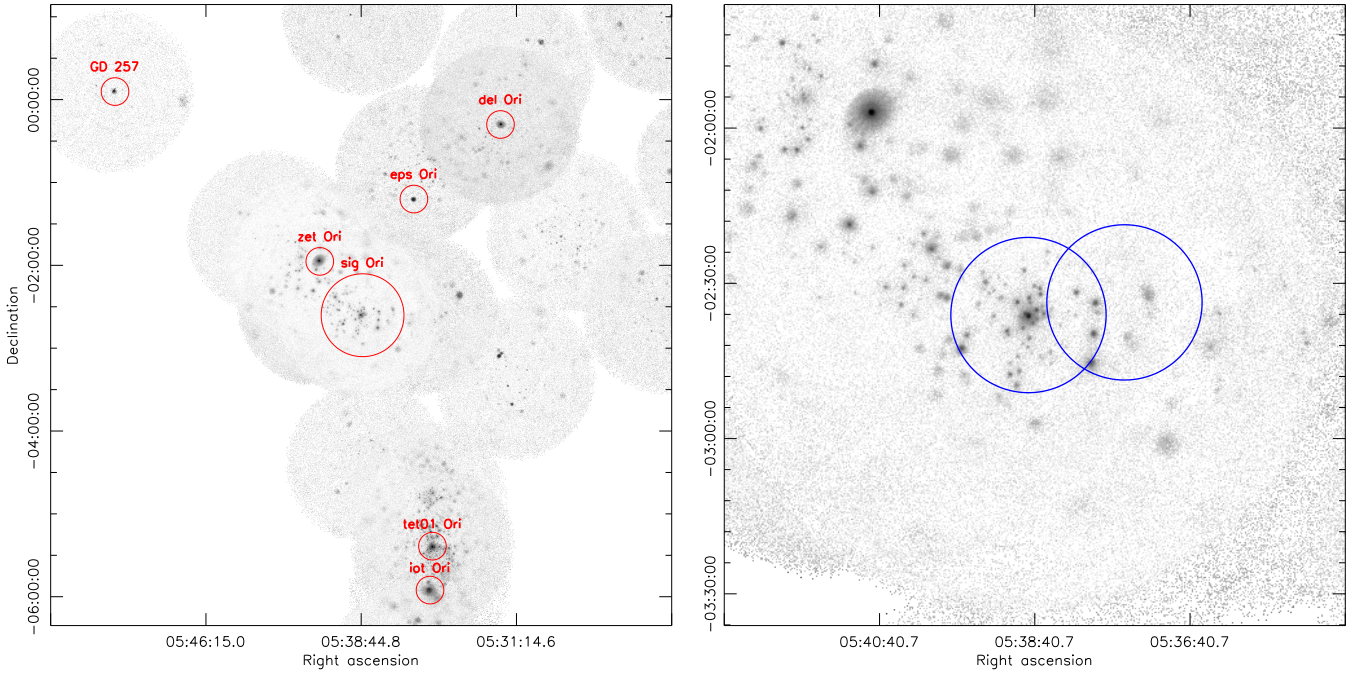

Fig. 1. Position Sensitive Proportional Counters (PSPC) 2.0 deg cut-off, intensity-scaled, summed pointed observations with *ROSAT* (0.1–2.4 keV) centred on the Trapezium-like system σ Ori. North is up and east is left. *Left:* the Orion Belt, to the centre and north, and the Orion Nebula Cluster, to the south (~7×7 deg^2). The brightest Orion complex stars in the area and the field white dwarf GD 257 are indicated and labelled. *Right:* zoom of the inner part (~2×2 deg^2). Circles represent the two regions observed by *XMM-Newton*: the first is centred on σ Ori and was analyzed by Franciosini et al. (2006); the second is centred on S Ori 55 and is analyzed in this work. Note the three X-ray sources of approximately the same brightness, aligned in the north-south direction, at about 15 arcmin to the west of σ Ori. Colour versions of all our figures are available in the electronic publication.

stars in the σ Orionis cluster was carried out by Wolk (1996) using *ROSAT*. His work was surpassed, however, by the exhaustive analysis of the full EPIC/*XMM-Newton* field centred on σ Ori AF–B by Franciosini et al. (2006). They detected 175 X-ray sources, 88 of which they identified with σ Orionis cluster members and candidate members. Franciosini et al. (2006) found no significant difference in the spectral properties of 23 classical and weak-line T Tauri stars classified in the literature. The formers, however, tended to be less X-ray luminous than the last. This trend was also found in the cluster centre by Caballero (2007b) using *Chandra* data, which confirmed, for instance, the earlier results by Neuhäuser et al. (1995) in Taurus. Additional intermediate- and low-mass stars with X-ray emission found with *Einstein*, the *Advanced Satellite for Cosmology and Astrophysics* (*ASCA*), *ROSAT*, and *Chandra* have been tabulated by Alcalá et al. (1996), Nakano et al. (1999), Adams et al. (2004), Caballero (2007a, 2008c), and Skinner et al. (2008). The X-ray variability of 23 young stars (and one galaxy) with *ROSAT* has been recently investigated by Caballero et al. (in prep.).

The X-ray activity extends down to below the hydrogen burning mass limit in σ Orionis. Mokler & Stelzer (2002) firstly investigated the X-ray emission near the substellar limit of the cluster. Of the seven very low-mass σ Orionis members in the error box of a *ROSAT* source, three of them were classified as unambiguous detections. However, two of the actual emitters are very close (ρ ~ 4–5 arcsec) to young low-mass cluster stars, that are probably the actual X-ray sources and not the brown dwarfs (Caballero 2006; Caballero et al. 2007). The third X-ray brown dwarf candidate in Mokler & Stelzer (2002), Mayrit 633059 (S Ori 3), is ΔJ ~ 1.2 mag brighter than the stellar/substellar boundary (i.e. it is a star).

To date, there remain only three *confirmed* σ Orionis brown dwarfs with X-ray emission (Franciosini et al. 2006): Mayrit 433123 (S Ori 25), Mayrit 487350 ([SE2004] 70), and Mayrit 396273 (S Ori J053818.2–023539). The spectra of the three of them have Li I λ6707.8 Å in absorption and/or low gravity features (e.g. abnormal alkali strength). Mayrit 433123 is a well known T Tauri substellar analog with Hα in strong emission, as well as He I (Béjar et al. 1999; Barrado y Navascués et al. 2003; Muzerolle et al. 2003). It is, besides, one of the very few brown dwarfs whose rotational velocity corrected from inclination has been derived (v = 14 km s^{-1}; Caballero et al. 2004). Mayrit 487350 underwent a flare during Franciosini et al. (2006)'s observations, and might be the primary of the widest exoplanetary system detected so far (r ~ 1700 AU; Caballero et al. 2006). Finally, Mayrit 396273 (the faintest brown dwarf of the trio) has been poorly investigated (Kenyon et al. 2005; Maxted et al. 2008).

With the aim of exploring the X-ray emission of extremely low-mass σ Orionis members, F. Mokler conducted new deep *XMM-Newton* observations to the west of the cluster, complementing Sanz-Forcada et al. (2004) and Franciosini et al. (2006)'s observations, that imaged the cluster centre. The new observations were centred, in its turn, on Mayrit 1158274 (S Ori 55), a substellar object at the brown dwarf/planet boundary with strong variable Hα emission and infrared flux excess longwards of 5 μm (Zapatero Osorio et al. 2002a; Zapatero Osorio et al. 2007; Luhman et al 2008).

We use the deep *XMM-Newton* observations to the west of the σ Orionis cluster to determine general X-ray properties of the young stars in the cluster external region, where the stellar density drops. To complete our work, we give upper limits to

Table 1. Basic data of the observations and reduction.

	Observations
Telescope	*XMM-Newton*
Instrument	EPIC
Cameras	PN+MOS1+MOS2
Mode	Full frame imaging
Filter	Thin
Centre α (J2000)	05 37 31.4
Centre δ (J2000)	−02 33 41
Start observations (UT)	2003 08 30, 13:52
End observations (UT)	2003 08 31, 09:02
PN exposure time	42 ks
MOS1 exposure time	50 ks
MOS2 exposure time	52 ks
Total duration	69 ks

the X-ray emission of the brown dwarfs in the field. Our intention is to determine the properties of the cluster X-ray emitters down to the substellar boundary. Once identified the X-ray stellar sources in the field, we conduct a spectral analysis to derive their basic parameters (e.g. energies of the thermal components, coronal metallicities, hydrogen column densities). We also look for flares during the X-ray monitoring and long-term variability. Finally, we complement our results with data from the literature to study the relation between X-ray emission and red optical-near infrared colours, which are indicative of spectral type and of the presence of surrounding discs.

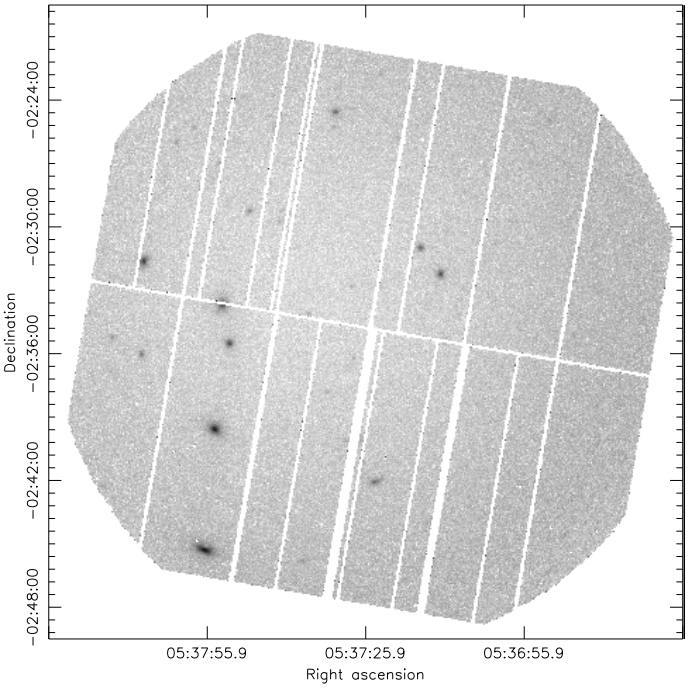

Fig. 2. Combined EPIC image of the western region of the σ Orionis cluster in the 0.3–7.5 keV energy band. The three aligned X-ray sources in right window in Fig. 1 are now splitted into four ones (the northernmost source falls just on a gap between detectors).

2. Observation and reduction

This *XMM-Newton* observation of the western region of the σ Orionis cluster (ID 0148300101) was performed in the revolution 682, between 2003 August 30 and 31, for a total duration of 69 ks. The three European Photon Imaging Cameras (EPIC) were operated simultaneously in full frame mode. In Table 1, we give the most important details of the observation.

Data reductions followed the standard procedures. We used the version 7.1.0 of the *XMM-Newton* Science Analysis System software (SAS) to derive a table of calibrated events. Then, we applied different filters to eliminate bad events and noise. Finally, high flaring background periods were removed in each detector separately to maximize the signal-to-noise ratio of weak sources. Although the observation was strongly affected by high background, the final effective exposure times (42, 50, and 52 ks for the PN, MOS1, and MOS2 detectors, respectively) are still longer than the observation analysed by Franciosini et al. (2006). Nevertheless, both observations are complementary since they slightly overlap at the eastern edge of our survey area.

In Fig. 2, we show the combined (filtered and calibrated) EPIC (PN+MOS1+MOS2) image. We created images in the chosen energy band (0.3–7.5 keV) for each detector individually. Then, we constructed exposure maps using the EEXMAP routine in the SAS software. These maps contain the spatial efficiency of the instruments. By dividing the images by the exposure maps, we corrected them for the quantum efficiency, filter transmission, and mirror vignetting. The resultant images were divided by the corresponding effective area to account for the difference in efficiency of the EPIC-PN and EPIC-MOS detectors. Finally, the task EMOSAIC was used to construct a combined PN+MOS image. A false-colour image combining X-ray, optical, and near-infrared data is shown in Fig. A.1.

3. Analysis and results

3.1. X-ray source detection

Standard packages available in SAS were used to reveal the sources in this region. In particular, we made use of the multitask EMLDETECT, that first performs a *sliding cell detection* and then uses a *maximum likelihood method* to derive parameters for each source. The sliding cell method consists in a simple sliding-window-box detection algorithm. We used a low signal-to-noise ratio above the background ($\sim 4\sigma$) to allow the detection of as many sources as possible. The list of sources is given, in its turn, as an input in the maximum likelihood method. Final derived parameters of EMLDETECT for each source are: total source count-rate (*CR*), likelihood of detection (*L*), and hardness ratio (*HR*). The reader is referred to the specific SAS documentation page[1] for more details on the procedure.

We performed the source detection for each camera dataset in three different energy bands: soft (0.3–2.0 keV), medium (2.0–4.5 keV), and hard (4.5–7.5 keV). Cleaned event-file corrected images (from bad pixels and noise) were used at this stage (see Section 2). We ignored the energy channels below 0.3 keV, because of the strong noise affecting the EPIC detectors under this value, and those above 7.5 keV, since only background is present at high energies. The energy bands selected here are very similar to those used in the *XMM-Newton* Bright Serendipitous

[1] http://xmm.vilspa.esa.es/sas/7.1.0/doc/emldetect/index.html.

Fig. 3. False-colour composite images centred on four representative X-ray sources (indicated with a 10 arcsec-radius circle): NX 5 (*top left*), NX 11 (*top right*), NX 30 (*bottom left*), and NX 32 (*bottom right*). DSS-2 plates at photographic $B_J R_F I_N$ bands are for blue, green, and red colours, respectively. Size is about 1.5×1.5 arcmin^2. North is up, east is left. In the NX 5 (OriNTT 429 AB) field, note the photometric cluster member candidate Mayrit 1416280 (OriNTT 429 C; Caballero 2008c) at $\rho \sim 12.1$ arcsec to the north of the spectroscopic binary. In the NX 11 field, the 2MASS and DENIS photo-centroids of the two objects discussed in the text are at ∼4 arcsec to the X-ray source. NX 30 (Mayrit 783254) is a young, early K-type dwarf with lithium in absorption. NX 32 (2E 1456) is a galaxy with a strong X-ray emission (Section 3.2.3). **Note: images are available only in the A&A version.**

Survey (XBSS; Della Ceca et al. 2004)[2]. The hardness ratios constructed using these bands,

$$HR_1 = \frac{CR_{\rm medium} - CR_{\rm soft}}{CR_{\rm medium} + CR_{\rm soft}} \quad (1)$$

$$HR_2 = \frac{CR_{\rm hard} - CR_{\rm medium}}{CR_{\rm hard} + CR_{\rm medium}}, \quad (2)$$

showed up as a very powerful tool to separate stellar sources from extragalactic ones. Non-absorbed coronal sources show, in general, low hardness-ratios ($HR_1 \lesssim -0.75$), while active galactic nuclei (AGNs) of galaxies present higher values because of both their high intrinsic absorption and emission mechanisms.

After a careful visual inspection of the sources in the initial list, which allowed us to reject artifacts (bad pixels in the gaps between chips and near the borders, multiple detections, and cosmic rays), we kept 41 X-ray sources with a maximum likelihood parameter $L \geq 15$. This parameter is defined as the Neperian logarithm of the probability P that the observed counts come from random Poissonian fluctuations ($L = -\ln P$). Therefore, we kept those sources with a probability $P \lesssim 3.0 \times 10^{-7}$ of being spurious (non-Poissonian effects –e.g. unidentified artifacts– may affect this probability when $L \sim 15$).

The final list of X-ray sources is given in Table A.1. For each source we give its position in equatorial coordinates, maximum likelihood of detection, count-rate obtained in each detector in the merged energy band 0.3–7.5 keV, and the hardness ratios (HR_1 and HR_2). Several sources fell in CCD gaps or in non-overlapping fields of view of the three cameras, and lack, as a result, some measurements. Six X-ray sources (NX 4, 8, 16, 25, 31, and 35) are detected only in one camera, and with maximum likelihood parameters in the interval $15 \leq L \leq 24$, which calls its truly emission into question.

3.2. Cross-identification and source classification

First, we looked for optical and near-infrared counterparts of the X-ray sources in the USNO-B1, DENIS, and 2MASS catalogues (Epchtein et al. 1997; Monet et al. 2003; Skrutskie et al. 2006) using Aladin (Bonnarel et al. 2000). The maximum positional offset allowed for an object to be declared a *possible* counterpart was fixed at a conservative value of 10 arcsec, bearing in mind

[2] The HR_2 and HR_3 hardness ratios in Della Ceca et al. (2004) are identical to our HR_1 and HR_2 ones, except for our soft band extending down to 0.3 keV instead of 0.5 keV.

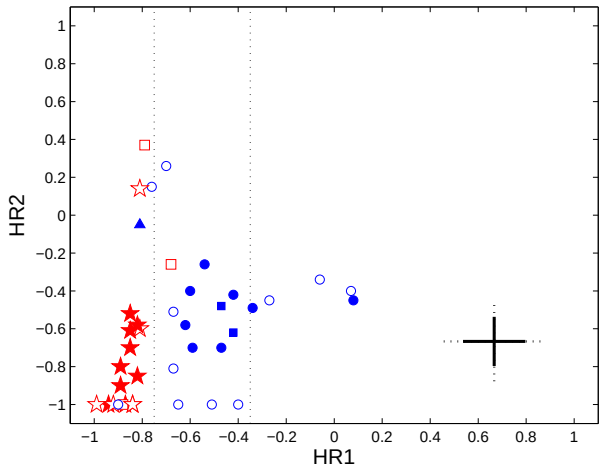

Fig. 4. Hardness ratios diagram (HR_2 vs. HR_1; compare with fig. 5 in Della Ceca et al. 2004). The different marker symbols represent: confirmed young stars in the Mayrit catalogue (–red– filled star symbols), candidate young stars (–red– open star symbols), field stars (–red– open squares), galaxies with near infrared and/or optical counterpart (–blue– filled circles), galaxies without near infrared or optical counterpart (–blue– open circles), NX 11 (–blue– filled up-triangle), and NX 23 and 41 (–blue– filled squares). The dotted lines at constant HR_1 correspond to the locus enclosing ∼90 % of type-1 AGNs in the *XMM-Newton* bright serendipitous survey sample (Della Ceca et al. 2004). In the lower right corner we report the median (solid) and the 90 % (dashed) percentile of the HR_1 and HR_2 errors.

the point-spread-function (PSF) of the EPIC cameras and their astromeric accuracy. For these cameras, the 80% of the PSF is contained in a circle with a diameter of 15 arcsec. For additional values of angular separations between X-ray and near-infrared counterparts in σ Orionis, see Franciosini et al. (2006). The mean offset between *XMM-Newton* and 2MASS/USNO-B1 positions for the 30 X-ray sources with near-infrared/optical counterparts and their standard deviations are $\Delta\alpha = -2.2 \pm 1.8$ arcsec, $\Delta\delta = -1.7 \pm 1.4$ arcsec (i.e. the X-ray sources are situated, on average, at 1.2σ to the southwest of the near-infrared/optical counterparts). The non-zero offset is, however, very small and does not affect our results. The majority of the near-infrared/optical counterparts of our sources are inside a radius of 5 arcsec. This value has been typically used as a good estimation of the effective ∼ 90% confidence radius of uncorrected positions (e.g. Watson et al. 2003). Note that the statistical error-circle for a faint XMM-Newton source has $\sigma_{\rm stat}$ = 1–2 arcsec.

The results of our cross-correlation are provided in Table A.2. We compiled equatorial coordinates, B_J (USNO-B1), i (DENIS), and $JHK_{\rm s}$ (2MASS) magnitudes (or lower limits), and alternative names of the 41 X-ray sources. Coordinates were taken from Tycho-2, 2MASS, or USNO-B1 (with this order of preference). For the three brightest stars in the sample, we give Tycho-2 B_T magnitudes (Høg et al. 2000) instead of photographic B_J, which is the average of the two USNO-B1 measurements ("$B1$" and "$B2$"). Uncertainties of the B_J and i magnitudes are ∼ 0.5 and 0.2–0.3 mag in this particular area. See also Caballero (2008c) for a discussion on the validity of the DENIS i-band magnitude when $\delta i = 1.00$ mag. Fig. 3 shows the optical counterparts of four representative X-ray sources and illustrates the cross-identification.

Up to eleven X-ray sources have no optical or near infrared counterpart at less than 12 arcsec; the nearest optical neighbours to some of these X-ray sources are located at more than 30 arcsec (40 arcsec for NX 25). For them, we provide the lower limits of their magnitudes from the completeness magnitudes of each survey. Besides, five X-ray sources have no 2MASS counterpart at 1.2–2.2 μm, but are catalogued by USNO-B1. Of them, only one source, NX 12, was also identified by DENIS at the *i* band. We list I_N instead of *i* in Table A.2 for sources NX 3 and NX 18, that were found at the three photographic bands ($B_J R_F I_N$). The remaining 25 X-ray sources have USNO-B1, DENIS, *and* 2MASS counterparts at less than $\sim$ 6 arcsec. Actually, the source NX 11 has *two* possible optical/near infrared counterparts (see Fig. 3); it will be discussed below.

We have classified the 41 X-ray sources and their corresponding optical/near infrared counterparts into young stars (15), field stars (4), galaxies (19), and sources of unknown nature (3) depending on their positions in the hardness ratio (Fig. 4), colour-colour, and colour magnitude (Fig. 5) diagrams, and on spectroscopic, astrometric, infrared photometric, and point spread function (PSF) information. Table 2 summarizes our classification. The last column indicates the Mayrit number for σ Orionis cluster members and candidates (Caballero 2008c).

3.2.1. Young stars

This class comprises the optical/near infrared counterparts of stars with known features of youth or that follow the spectrophotometric sequence of the σ Orionis cluster. We have splitted the 15 young stars, in its turn, into confirmed (8) and candidate young stars (7). Six of the eight confirmed young stars have Li I λ6707.8 Å in absorption in spectra taken by Lee et al. (1994), Wolk (1996), and Caballero (2006): NX 5, 7, 20, 27, 28, and 30 (NX 5, 27, and 28 have redundant detections). There is information on its Hα λ6562.8 Å line for the six stars. In all cases, the Hα emission seems to be chromospheric. Likewise, other two stars (NX 36 and 38) have both intense Hα emission detected with prism-objective and Schmidt plates (Wiramihardja et al. 1989, 1991) and infrared flux excess at the IRAC/*Spitzer* bands (Hernández et al. 2007) These effects are ascribed to the presence of circumstellar discs from where the central object accretes material. The two objects have been classified as classical T Tauri stars (class II).

There remain seven young star candidates. Four of them were tabulated as photometric cluster member candidates by Wolk (1996), Scholz & Eislöffel (2004), Sherry et al. (2004), and Caballero (2006, 2007a): NX 4, 17, 34, and 37. The last star appears in catalogues prepared with *Einstein* data (Habing et al. 1994), was classified as a pre-main sequence *ROSAT* X-ray emitter star by Wolk (1996), and had a large unabsorbed X-ray luminosity (L_X = 30.66 [cgs]) in the *XMM-Newton* observations by Franciosini et al. (2006), that make NX 37 to be a truly young active star. Caballero (2006) obtained a poor optical spectrum of NX 17 where the Li I and Hα lines were hardly discernible. The three remaining photometric candidates (NX 14, 16, and 21) are presented here for the first time. The three of them also follow the sequence of the young stars in the hardness ratio, colour-colour, and colour-magnitude diagrams. In reallity, they are slightly bluewards of the conservative selection criterion in the *i* vs. $i - K_s$ diagram in fig. 4 in Caballero (2008c), but still redwards of the lower envelope of confirmed young stars in σ Orionis. As already mentioned by Caballero et al. (2006), cluster members with X-ray emission tend to have bluer optical/near-infrared colours than T Tauri analogs. Since most of the photometric searches in the cluster have been based on colour-magnitude diagrams and, therefore, biased towards the detection of (red) T Tauri analogs, the bluest part of the spectrophotometric cluster sequence is not well defined yet and many X-ray stars still wait identification. All the 15 young stars and candidates have hardness ratios $HR_1 < -0.75$.

3.2.2. Field stars

The four field star candidates have hardness ratios consistent with their probable stellar nature if uncertainties are taken into account. The brightest counterpart (NX 21) is a Tycho-2 star with accurate astrometry that was classified as a non-cluster member by Caballero (2007a) based on its proper motion larger than 10 mas a^{-1}. Their colours match with those of F-type (interacting binary?) dwarfs. It is the only field star whose maximum likelihood parameter *L* is larger than 25.

The remaining three field star candidates, that are among the faintest X-ray sources in our sample, are presented here for the first time. They have very blue $i - K_s$ colours for its *i* magnitude if compared with the σ Orionis sequence in the colour-magnitude diagram (by up to 0.75–1.00 mag), but follow the dwarf sequence in the colour-colour diagram (Fig. 5). They seem to be late K-type dwarfs in the foreground of σ Orionis.

3.2.3. Galaxies

The eleven X-ray sources without optical or near infrared counterpart are probably background galaxies. First, they have magnitudes $J \gtrsim 17.1$ mag, that correspond to the lower mass part of the substellar domain in σ Orionis (Caballero et al. 2007). If cluster members, they would have magnitudes $i \gtrsim 21$ mag, which would explain their null detection in the optical. However, even in the most favourable case of an α index of the mass spectrum ($\Delta N/\Delta M \propto M^{-\alpha}$) close to the Salpeter one (α = –2.35), which is in clear contradiction with recent determinations of the initial mass function in the cluster (Caballero et al. 2007), we would not expect such a large population of faint cluster members. Secondly, these hypothetical faint cluster members would have extraordinary large L_X/L_{bol} ratios: the faintest X-ray brown dwarfs in σ Orionis (Section 1) are brighter than J = 15.5 mag. Thirdly, the great majority of the X-ray sources have hardness ratios $HR_1 > -0.75$, more typical of extragalactic sources. And finally, the contamination by background galaxies in σ Orionis, some of which may be X-ray emitters, gets more important at the faintest magnitudes. See compilations of extragalactic sources in the Orion Belt (some of which were previously identified as active stars) in Caballero (2008c), Caballero & Solano (2008), and Caballero et al. (2008). As a result, the abundance of X-ray sources with faint optical counterparts or without counterparts at all (see Table B.1 in Franciosini et al. 2006) is naturally explained by a background population of galaxies (especially, AGNs powered by massive black holes – Rees 1984; Stocke et al. 1991; Comastri et al. 1995; Alexander et al. 2003; Ueda et al. 2003).

The extragalactic hypothesis is supported by the identification of four X-ray sources in our field with extended PSFs in the optical and/or near-infrared (NX 10, 12, 13, and 32) and four USNO-B1 sources without near infrared counterpart. The last sources have colours $B_J - J \lesssim 2.7$ mag, i.e. bluer than late K-type stars, approximately. Such blue colours at the corre-

Table 2. Classification of X-ray sources.

NX	[FPS2006][a]	Remarks	Reference[b]	Class	Mayrit
1	...	No optical/nIR counterpart	...	Galaxy	...
2	...	No optical/nIR counterpart	...	Galaxy	...
3	...	Only optical counterpart	...	Galaxy	...
4	...	Phot. young candidate	Ca07a	Young star candidate	1456284
5	...	Li I, Hα, SB2	Lee94, Ca06	Young star	1415279AB
6	...	Blue $i - K_s$	...	Field star	...
7	...	Li I	Ca06	Young star	1374283
8	...	No optical/nIR counterpart	...	Galaxy	...
9	...	Blue $i - K_s$	...	Field star	...
10	...	Extended PSF	...	Galaxy	...
11	...	Extended PSF/binary system	...	Unknown	...
12	...	Extended PSF, only optical counterpart	...	Galaxy	...
13	...	Extended PSF, blue/red, strong X-ray	...	Galaxy	...
14	...	New phot. young candidate	...	Young star candidate	1149270
15	...	No optical/nIR counterpart	...	Galaxy	...
16	...	New phot. young candidate	...	Young star candidate	1344302
17	...	Phot. young candidate, Li I?, Hα?	Sh04, Ca06	Young star candidate	1298302
18	...	Only optical counterpart	...	Galaxy	...
19	...	Only optical counterpart	...	Galaxy	...
20	...	Li I	Sh04, Ca06	Young star	1027277
21	...	New phot. young candidate	...	Young star candidate	1160240
22	...	No μ	Ca07a	Field star	...
23	...	Blue $i - K_s$	...	Unknown	...
24	...	Blue $i - K_s$	...	Field star	...
25	...	No optical/nIR counterpart	...	Galaxy	...
26	...	No optical/nIR counterpart	...	Galaxy	...
27	1	Li I, Hα, M1-3	Wo06, Ca08c	Young star	797272
28	2	Li I, broad Hα, K0	Wo96, Ca06	Young star	789281
29	...	No optical/nIR counterpart	...	Galaxy	...
30	3	Li I, Hα, K0	Wo96	Young star	783254
31	...	No optical/nIR counterpart	...	Galaxy	...
32	...	Extended PSF, blue/red, strong X-ray	Ca08d	Galaxy	...
33	...	Only optical counterpart	...	Galaxy	...
34	...	Phot. young candidate	SE04, Sh04	Young star candidate	887313
35	5	No optical/nIR counterpart	...	Galaxy	...
36	7	Strong Hα, class II	Wi89, Sh04, He07	Young star	662301
37	8	Phot. young candidate, X-ray	Wo96, Fr06	Young star candidate	615296
38	9	Strong Hα, class II	Wi91, Sh04, He07	Young star	547270
39	12	No optical/nIR counterpart	...	Galaxy	...
40	...	No optical/nIR counterpart	...	Galaxy	...
41	14	Blue $i - K_s$	...	Unknown	...

[a] X-ray source number in Franciosini et al. (2006).
[b] Reference abbreviations – Wi89: Wiramihardja et al. (1989); Wi91: Wiramihardja et al. (1991); Lee94: Lee et al. (1994); Wo96: Wolk (1996); SE04: Scholz & Eislöffel (2004); Sh04: Sherry et al. (2004); Fr06: Franciosini et al. (2006); Ca06: Caballero (2006); Ca07a: Caballero (2007a); He07: Hernández et al. (2007); Ca08c: Caballero (2008c); Ca08d: Caballero et al. (2008).

sponding faint magnitudes are inconsistent with those of early-type stars at very long heliocentric distances (at several Galactic height scales; Chen et al. 2001) and with late-type dwarfs in the foreground of the cluster. The low extinction towards σ Orionis ($A_V \sim 0.3$ mag) cannot be responsible of the faintness of these sources in the near infrared.

Two of the galaxies with extended PSFs were early detected by *Einstein*: 2E 1448 (NX 13) and 2E 1456 (NX 32, the second brightest X-ray source in our sample). The NASA/IPAC Extragalactic Database (NED) tabulates isophotal major axes $2a = 24.0$ and 14.60 arcsec at the reference level 20.0 K_s-mag arcsec^{-2}, respectively. Both of them were catalogued as galaxies with peculiar colours by Caballero (2008c): on the one hand, NX 32 has very blue colours in the optical ($B_J - i \sim -0.3$ mag), but very red colours in the near infrared ($J - K_s = 1.68 \pm 0.10$ mag). On the other hand, NX 13 has appreciable emission at 4.5–8.0 μm (Hernández et al. 2007). In Section. 4.4 we present spectral fitting of these two galaxies.

3.2.4. Sources of unknown nature

NX 11. We have not been able to discriminate which is the actual source of the X-ray emission of NX 11. As mentioned in Section 3.2, NX 11 has *two* possible optical/near infrared counterparts. One is a dwarf star candidate (up-triangle in right window in Fig. 5) and the other one (down-triangle) is a red galaxy with an extended PSF. Both counterparts are at ~ 4 arcsec to the X-ray source. If the dwarf star were the X-ray emitter, it would be an active star in the field and not a σ Orionis member candidate.

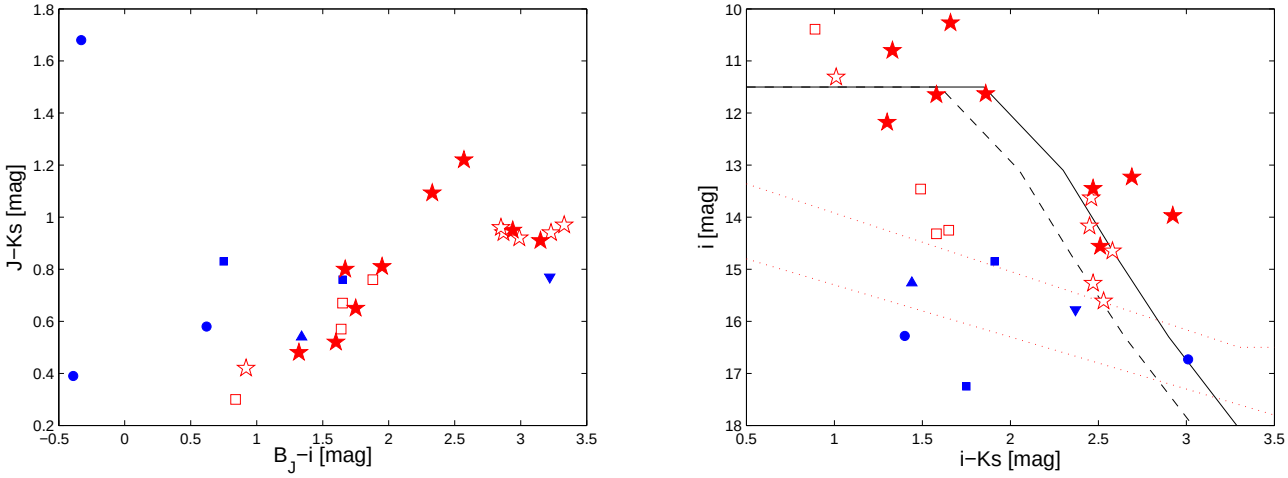

Fig. 5. Colour-colour and colour-magnitude diagrams. The marker symbols are as in Fig. 4. The (blue) filled up- and down-triangles are for the brighter and fainter (in B_J) counterparts of NX 11, respectively. *Left:* $J - K_s$ vs. $B_J - i$ colour-colour diagram. The star sequence runs from $(B_J - i, J - K_s) \sim (1.0, 0.4)$ mag to $\sim (2.5, 1.0)$ mag. At redder $B_J - i$ colours, the $J - K_s$ colours keep roughly constant at ~ 1.0 mag except for disc harbour stars, like the two class II stars at $(B_J - i, J - K_s) \sim (2.3–2.6, 1.10–1.25)$ mag. *Right:* i vs. $i - K_s$ colour-magnitude diagram. The dotted (red) lines are approximate completeness and detection limits of the combined DENIS/2MASS cross-correlation. The solid (black) line is the criterion for selecting candidate cluster stars and brown dwarfs without known features of youth in σ Orionis used by Caballero (2008c). The dashed (black) line is the criterion shifted bluewards by 0.25 mag.

NX 23. In spite of its clear detection in the PN, MOS1, and MOS2 cameras ($L = 79$), and its relative brightness in the optical and the near infrared (e.g. $J = 13.70 \pm 0.03$ mag), NX 23 displays the largest deviation between the coordinates of the X-ray and optical/near infrared counterparts ($\rho \sim 7$ arcsec). Besides, while the optical/near infrared counterpart have typical colours of normal field dwarfs, the hardness ratios are peculiar for its hypothetical stellar nature ($HR_1 = -0.42 \pm 0.11$, $HR_2 = -0.62 \pm 0.11$). To explain this dilemma, the origin of the X-ray source could be an X-ray emitter galaxy in the background that is not detectable in the Digital Sky Survey (nor DENIS nor 2MASS) instead of an irregular, extremely active, X-ray emission from the correlated dwarf.

NX 41. This X-ray source was previously identified with a possible cluster candidate from 2MASS by Franciosini et al. (2006; with identification number 14 in their list). However, it displays much bluer colours than confirmed σ Orionis members of the same magnitude ($J = 16.33 \pm 0.09$ mag, $i - K_s \sim 1.8$ mag), combined with soft hardness ratios ($HR_1 = -0.47 \pm 0.16$, $HR_2 = -0.48 \pm 0.16$). It is probably another active galaxy in the background.

3.3. Derivation of X-ray properties

Of the 15 X-ray sources cross-identified with σ Orionis members and candidate members in Section 3.2.1, twelve have more than 800 counts in the summed EPIC image after background correction. As a matter of a fact, all of them have maximum likelihood parameters $L \gtrsim 100$. Only three young stars (NX 4, 16, and 36) have X-ray emission faint enough for preventing the derivation of X-ray properties (i.e. less than about 400 counts, $L \lesssim 25$). We carried out a spectral analysis of the 12 brightest X-ray counterparts of young stars using data from the EPIC camera and the XSPEC spectral fitting package (Arnaud 1996, 2004). The X-ray spectrum of each one of these sources was first corrected by subtracting a background spectrum, extracted from a close region in the same detector and scaled to the source extraction region area. We adopted the Astrophysical Plasma Emission Database (APED; Smith et al. 2001), that contains the relevant atomic data for both continuum and line emission included in the XSPEC software. Interstellar absorption, N_H, was taken into account using the photo-electric absorption cross-sections of Morrison & McCammon (1983), also available in XSPEC.

In Table 3, we give the results of fitting with the Astrophysical Plasma Emission Code (APEC) model. In general, we used a two-temperature ($2T$) model, with fixed relative abundances. We applied a one-temperature ($1T$) model only for the four sources with maximum likelihood parameters $L \sim 100$ (i.e. less counts), since the addition of a second thermal component did not improve the χ^2 goodness-of-fit of the least-square solution. The remaining X-ray sources with satisfactory fitting to a $2T$ model have $L \gtrsim 750$ (and up to $L \sim 33\,000$). For source NX 27, a third thermal component was needed to obtain an accurate fitting to the hard tail of its X-ray spectrum (a power-law component cannot satisfactorily fit it). The temperatures and emission measure ratio given in the table correspond to the soft and medium thermal components. See further details in Section 4.1.3. In Figs. A.2 and A.3, we show the X-ray spectral fitting of the twelve young stars.

4. Discussion

4.1. X-ray young stars

4.1.1. New X-ray sources in σ Orionis

We have derived the X-ray properties of 12 young stars (Table 3), while three of them were too faint. Of the latter stars,

Table 3. X-ray properties of our 12 brightest X-ray sources associated to σ Orionis cluster members and candidates, with errors measured as the 90% confidence range.

NX	Mayrit	kT_1 [keV]	kT_2 [keV]	EM_1/EM_2	$Z/Z_\odot^a$	$N_{\rm H}$ [10^{21} cm^{-2}]	$\chi^2_{\rm red}$/(d.o.f.)	$F_{\rm X}^b$ [10^{-13} erg cm^{-2} s^{-1}]
5	1415279AB	$0.36^{+0.05}_{-0.04}$	$1.02^{+0.06}_{-0.06}$	0.77	$0.13^{+0.04}_{-0.03}$	$0.56^{+0.19}_{-0.17}$	0.98/155	$2.21^{+2.54}_{-2.12}$
7	1374283	$0.65^{+0.09}_{-0.16}$	$1.21^{+0.32}_{-0.73}$	1.16	$0.18^{+0.11}_{-0.07}$	$1.04^{+0.37}_{-0.17}$	1.27/98	$1.38^{+2.29}_{-1.14}$
14	1149270	$0.77^{+0.19}_{-0.15}$	...	....	$0.08^{+0.03}_{-0.03}$	$0.55^{+0.42}_{-0.31}$	1.07/22	$0.09^{+0.13}_{-0.03}$
17	1298302	$0.90^{+0.15}_{-0.11}$	$3.31^{+60.7}_{-1.18}$	0.36	$0.39^{+0.39}_{-0.14}$	$0.19^{+0.64}_{-0.19}$	0.92/76	$1.28^{+1.46}_{-1.02}$
20	1027277	$0.75^{+0.18}_{-0.44}$	...	...	$0.09^{+0.12}_{-0.09}$	$1.02^{+5.34}_{-0.81}$	1.04/34	$0.12^{+0.02}_{-0.02}$
21	1160240	$0.72^{+0.14}_{-0.16}$	...	...	$0.07^{+0.02}_{-0.02}$	$0.57^{+0.36}_{-0.27}$	0.89/42	$0.23^{+0.04}_{-0.05}$
27[c]	797272	$0.32^{+0.06}_{-0.04}$	$1.12^{+0.15}_{-0.12}$	0.84	$0.15^{+0.22}_{-0.08}$	$0.72^{+0.34}_{-0.22}$	1.22/198	$3.47^{+3.74}_{-2.77}$
28	789281	$0.75^{+0.03}_{-0.06}$	$1.77^{+0.18}_{-0.21}$	0.31	$0.38^{+0.12}_{-0.12}$	$0.46^{+0.16}_{-0.12}$	1.10/336	$7.07^{+7.76}_{-6.78}$
30	783254	$0.78^{+0.02}_{-0.02}$	$1.92^{+0.13}_{-0.17}$	0.60	$0.21^{+0.03}_{-0.06}$	$0.37^{+0.03}_{-0.06}$	1.33/354	$11.6^{+12.4}_{-11.4}$
34	887313	$0.45^{+0.27}_{-0.33}$	...	...	$0.03^{+0.10}_{-0.03}$	$1.18^{+5.67}_{-1.18}$	1.13/27	$0.31^{+0.39}_{-0.01}$
37	615296	$0.34^{+0.04}_{-0.03}$	$1.14^{+0.07}_{-0.10}$	0.63	$0.13^{+0.04}_{-0.03}$	$0.71^{+0.15}_{-0.15}$	0.99/270	$4.49^{+4.96}_{-4.10}$
38	547270	$0.67^{+0.10}_{-0.19}$	$1.30^{+0.42}_{-0.30}$	0.66	$0.51^{+0.84}_{-0.31}$	$0.17^{+0.07}_{-0.17}$	1.04/48	$0.56^{+0.74}_{-0.39}$

[a] Global abundance scaled on the solar value from Anders & Grevesse (1989).
[b] Unabsorbed X-ray flux in the 0.3–10.0 keV band. $F_{\rm X}$ was computed through fixing $N_{\rm H} = 0$ after fitting with XSPEC (using the APEC model). For details on the fitting procedure and how to calculate errors, we refer the reader to the online XSPEC guide (accessible from the HEASARC website: `http://heasarc.nasa.gov/docs/xanadu/xspec/index.html`).
[c] For source NX 27, a 3T model was also used. The third component has $kT_3 = 4.34^{+59.2}_{-1.57}$ keV and $EM_1/EM_3 = 1.01$.

– NX 4 is a bright Tycho-2 star with arguable X-ray emission and expected spectral type at around late-A or early-F (with low frequencies of X-ray emission),
– NX 16 is in the bluest part of the cluster sequence in the i vs. $i - K_{\rm s}$ diagram, has a very low maximum likelihood parameter ($L = 17$), and was only detected by one camera (i.e. its youth is debatable),
– and NX 36, with reliable (faint) X-ray emission and $J - K_{\rm s} = 1.22 \pm 0.04$ mag, is the reddest young star in our sample and one of the reddest stars in σ Orionis. The infrared flux excess at IRAC and MIPS/*Spitzer* passbands and its strong Hα emission (see references in Table 2) are an evidence of NX 36 (Mayrit 662301) having a developed disc, possibly edge-on, that absorbs any possible X-ray emission from the corona or from the channels that connect the inner border of the disc with the central object (Königl 1991).

Of the twelve young stars with derived X-ray properties, four have not enough signal – i.e. counts – for an accurate fitting to a 2T-model. Therefore, only one thermal component was fitted for the four of them. They are: NX 20 (a confirmed young star with lithium), NX 14 and NX 21 (two new photometric cluster member candidates), and NX 34 (a non-variable photometric cluster member candidate; Scholz & Eislöffel 2004). The X-ray emission ensures their extreme youth. Likewise, the set of eight young stars with at least two thermal components comprises six confirmed stars with spectroscopic features of youth (NX 5, 7, 27, 28, 30, and 38) and two previously known photometric cluster member candidates (NX 17 and 37).

To sum up, by deriving their X-ray properties, we show that five young star candidates selected in colour-magnitude diagrams are actually young (two are presented here for the first time –NX 14 and 21–; two were unconfirmed cluster member candidates –NX 17 and 34–; one was confirmed by Franciosini et al. (2006) –NX 37–). Besides, we first find X-ray emission from three young stars with lithium (NX 5, 7, and 20). In other words, of the 15 young stars investigated here, the detection of X-ray emission of *nine* of them is new (but NX 4 and 16 detections are questionable).

Although these numbers are far from the numerous population of X-ray sources first found in the trailblazer works by Wolk (1996) and Franciosini et al. (2006), some of our young stars with emission are at previously uncovered angular distances from the cluster centre. Using previous *ROSAT* and *XMM-Newton* data, they could properly study the innermost 15 arcmin of σ Orionis, and hardly in the 15–20 arcmin external region. However, as shown by Caballero (2008a), the "core" and the "halo" of the cluster extends up to 20 and 30 arcmin, respectively. At larger separations from the Trapezium-like system that defines the cluster centre (i.e. $\rho > 30$ arcmin), the surface density of cluster members drops notoriously, and the contamination by nearby young populations (around Mintaka to the northeast, Alnilam to the northwest, and the Horsehead Nebula to the southeast) gets important (Jeffries et al. 2006; Caballero 2008c). Except for NX 34 (that is at $\rho \sim 14.8$ arcmin from σ Ori AF–B), all our X-ray young stars lie on the external (17 arcmin $\lesssim \rho \lesssim$ 24 arcmin) region (i.e. in the cluster core-to-halo transition). The decrease in the surface density of X-ray young stars at large distances from the cluster centre that we observe is an obvious consequence of the decrease in the surface density of σ Orionis members, that approximately follows a distribution proportional to ρ^{-1} (Caballero 2008a).

4.1.2. Discs and $N_{\rm H}$

The value of the column density $N_{\rm H}$ in our X-ray model accounted for both the interstellar column density and the circumstellar material that could surround each star, like a protoplanetary disc or diffuse interstellar material left over

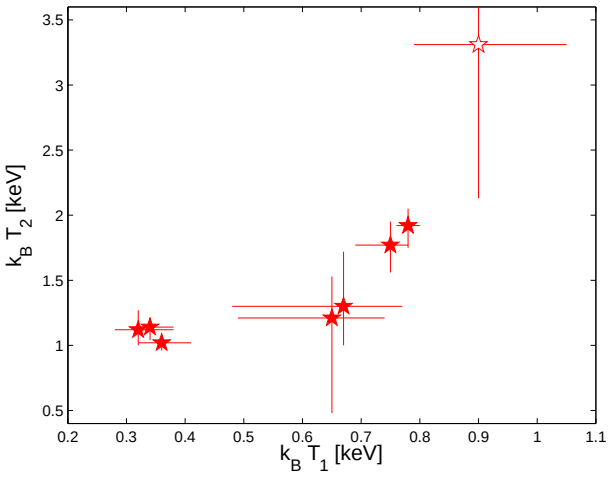

Fig. 6. Same as Fig. 5, but for the k_BT_2 vs. k_BT_1 diagram only for the young stars in Table 3. The young star candidate with high temperatures is NX 17. Its upper limit of k_BT_2 is undetermined.

from its formation. On the one hand, from the low $E(B-V)$ colour excess towards the σ Orionis cluster, that lies in the interval 0.04–0.09 mag (Lee 1968; Béjar et al. 2001; Béjar et al. 2004; Hernández et al. 2005; Sherry et al. 2008; González-Hernández et al. 2008), it is derived that the expected interstellar column density approximately varies between 2.2 and 4.9 10^{16} m^{-2} (i.e. $N_{\rm H} \approx 0.22$–0.49 10^{21} cm^{-2}). There are two of our 12 young stars with $N_{\rm H}$ larger than this range ($N_{\rm H} \approx 1.0 - 1.2 \times 10^{21}$ cm^{-2}), even taking the errors into account. They are NX 7 ($J - K_{\rm s} = 0.48 \pm 0.03$ mag) and NX 34 ($J - K_{\rm s} = 0.96 \pm 0.05$ mag). There are no hints for the first star to have a disc (NX 7 falls out of the area investigated to date with the *Spitzer Space Telescope* and the Infrared Array Camera; Hernández et al. 2007), while the relatively red colour for the magnitude of the second star might suggest the presence of a disc (NX 34 has the third reddest $J - K_{\rm s}$ among the 12 stars).

On the other hand, there are two σ Orionis stars in our analysis catalogued as classical T Tauri stars. One is the faint X-ray emitter NX 36, that was discarded for the spectral energy distribution fitting because of their low number of summed counts. Its very red near-infrared colours ($J - K_{\rm s} = 1.22 \pm 0.04$ mag) support the scenario of an X-ray absorbent disc (Section 4.1.1). However, the other classical T Tauri star with infrared flux excess at 2–8 μm (NX 38, with colour index $J - K_{\rm s} = 1.10 \pm 0.04$ mag) has a *low* value of $N_{\rm H}$. There are four young stars whose X-ray parameters have been derived and possess less counts than NX 38, and none of them displays such a $J - K_{\rm s}$-$N_{\rm H}$ incompatibility. Instead of claiming a contradiction with the scenario of an X-ray absorbent disc, we propose a simpler solution based on a geometrical fact: the X-ray emission from the upper layers of the atmosphere of NX 38 passes through a shorter portion of disc because of a relatively larger inclination angle with our visual (i.e. the disc is pole-on). This hypothesis, nevertheless, should be verified by determining the disc inclination angle.

4.1.3. X-ray variability

In the source detection stage (Section 3.1), we created a *cleaned* event-list, rejecting 30 % of the observation (see Table 1). We used this event-list to look for variations in the lightcurve of our sources. Since the period in which high background level is present is large, the statistical analysis of variations was not possible. In these conditions, it is difficult to detect, for instance, variations due to rotational modulation. In our sample, two sources showed clear flaring events in their lightcurves: NX 17 and NX 27 (see Fig. 7). In this section, we focus on such events.

NX 17. This source (identified with the young cluster member candidate Mayrit 1298302; see Table 2) showed a large flare with a duration of more than 4 h and a relative increase in flux of $\sim$ 30. This is much larger than observed in young stars in Taurus (Franciosini et al. 2007) and comparable with those observed in some young stellar objects in the Orion Nebula Cluster (Favata et al. 2005). The mean coronal temperature during the observation reached 3.3 keV ($T \sim 38$ MK). This value is typical of high-energy flaring events in late-type stars (see Crespo-Chacón et al. 2007, and references therein).

NX 27. This source has been identified with the σ Orionis member Mayrit 797272, an M1–3 type star that shows a large lithium absorption line (Wolk 1996; Caballero et al. 2008). In its X-ray lightcurve, it showed a first flare at $t \approx 14$ ks from the beginning of the observation and high variability during the second half of it, probably coming from a second flare. With a total duration of $\sim$ 9 ks, the first flare presented a relative increase in flux of $\sim$ 4, similar to the observed in other young stars (e.g. Favata et al. 2005; Franciosini et al. 2007) and in field M dwarfs (e.g. Robrade & Schmitt 2005). The temperature of the hotter component in the spectral fitting to the whole observation is 4.3 keV ($T \sim 50$ MK). Both flares are probably contributing to the spectra.

4.2. Young stars and brown dwarfs without X-ray counterpart

A series of star and bright brown dwarf members and candidates of the σ Orionis cluster in the Mayrit catalogue (Caballero 2008c), and that fall in the area covered by *XMM-Newton*, were not detected in this observation because of their low X-ray emission. Most of them show features of youth, such as Li I in absorption, Hα in strong broad emission, abnormal strength of alkali lines due to low gravity, early spectral types (OB), and/or flux excess longwards of the J band (i.e. class II). S Ori 55 (Section 1), located in the centre of the field of view and close to the central gaps, is one of these objects. Other interesting ones are S Ori 70 (see, again, Section 1), with a tentative mass of $\sim 3\,M_{\rm Jup}$ and a possible disc, and S Ori 66, also in the planetary-mass domain and with a (likely) mid-infrared flux excess and strong Hα emission (Barrado y Navascués et al. 2001; Zapatero Osorio et al. 2008; Scholz & Jayawardhana 2008; Luhman et al 2008). They are maybe the most interesting ultra low-mass objects in the area. Some other candidates and members of the cluster fall in a detector gap or close to the border, which avoided any reliable detection of such sources.

For all the members and candidates of σ Orionis in the Mayrit catalogue with no X-ray counterpart in our observation, we give upper limits to their X-ray emission in Table A.3. Fluxes were determined from the count-rate measured in a circular region of 15 arcsec centred on the position of each source in the (exposure-map corrected) EPIC image. The count-rate simula-

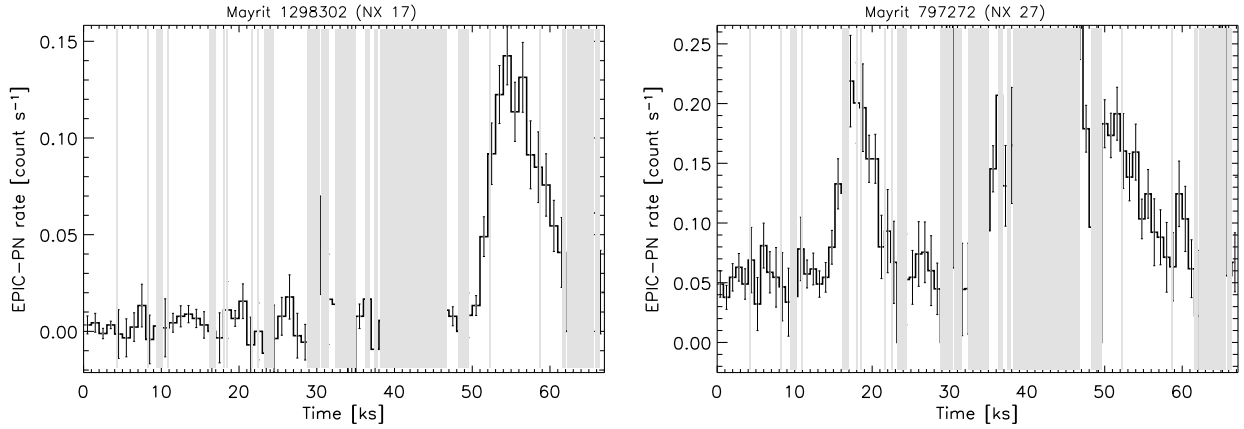

Fig. 7. Background subtracted X-ray lightcurves of the stars Mayrit 1298302 (NX 17) and Mayrit 797272 (NX 27) in the energy range 0.3–7.5 keV. The bin size is 800 s. The light grey area marks the parts of the spectrum rejected for this study because of the high background level. Both stars showed clear flaring events which caused the rising of the coronal temperature (see text for details).

tor WebPIMMS[3] was used to transform count-rates to fluxes. We assumed a hot plasma model with $kT = 1$ keV and a column density $N_{\rm H} = 0.27 \times 10^{21}$ cm^{-2} for every source (see Section 4.1.2 for a detailed discussion on the interstellar column density in the direction of the σ Orionis cluster). The temperature of 1 keV is representative of the corona of young stars and has been also observed in the X-ray emitting brown dwarfs in the Orion Nebula cluster (Feigelson et al. 2005). Some of the listed objects were marginally detected by the detection algorithm, but showed maximum likelihood parameters below the value chosen here for reliable detection, $L \geq 15$.

The upper limits given here put constraints to the X-ray emission of the low mass objects in the field. Very few is known about the X-ray emission from brown dwarfs. Apart from the σ Orionis brown dwarfs introduced in Section 1, there have been only a handful of detections in other young star-forming regions, such as the Orion Nebula Cluster, Chamaeleon, and Taurus (Neuhäuser & Comerón 1998; Neuhäuser et al. 1999; Imanishi et al. 2001; Tsuboi et al. 2003; Preibisch et al. 2005). There have also been reports of X-ray emission from a brown dwarf in the Pleiades (Briggs & Pye 2004) and two brown dwarfs in the field: LP 944–20 (member of the Castor moving group, Rutledge et al. 2000) and GJ 569B[ab] (questionable; Stelzer 2004). Nowadays, it is accepted that brown dwarfs and low-mass stars share the same formation mechanism (e.g. Caballero et al. 2007) and, therefore, brown dwarfs are "stars to scale" without stable hydrogen burning. Albeit brown dwarfs are smaller (fainter, cooler) than stars, they rotate much faster (with periods of about 10 h; see Mohanty & Basri 2003, and references therein) which may enhance their magnetically-driven, internal dynamos. This enhancement might produce, in its turn, an extra heating of the hot, tenuous, X-ray-emitting, upper atmospheric layer in brown dwarfs.

4.3. Comparison to previous XMM-Newton observations

There are nine X-ray sources in common with the *XMM-Newton* observations by Franciosini et al. (2006) and ours (see second column in Table 2). They are six young stars, two galaxies (NX 35 and 39), and a source of unknown nature (NX 41; Section 3.2.4), classified by Franciosini et al. (2006) as σ Orionis cluster members or candidates, unidentified X-ray sources, and a possible cluster candidate from 2MASS, respectively. The X-ray parameters determined here for the stellar sources for which a spectral fitting was possible in both works (NX 28, NX 30, and NX 37) are well in agreement with those obtained by Franciosini et al. (2006). The remaining stars in common are too faint in, at least, one of both works to perform a robust fitting to their spectra and, thus, we cannot compare results. The case of NX 27 ([FPS2006] 1 in Franciosini et al. 2006) is remarkable since, in our observation, its count-rate is more than one order of magnitude higher than in the Franciosini et al. (2006)'s one. Here, the star showed high X-ray variability coming from large flaring events (Section 4.1.3) and it had counts enough to do an accurate spectral fitting. The energy band used in our study, 0.3 – 7.5 keV, is similar to that of Franciosini et al. (2006), who used 0.3 – 8.0 keV.

Besides, there are seven additional X-ray sources that Franciosini et al. (2006) associated to cluster members and candidates and that were not detected with our task, although they fall in our survey area. However, all of them (with [FPS2006] identification number in the last column of Table A.3) are very faint and located in (or very close to) borders or gaps of the detectors in our observation.

4.4. X-ray galaxies

Of the 12 X-ray sources in Table A.1 with maximum likelihood parameters $L \gtrsim 400$, eight are young stars and four are background galaxies with $HR_2 > -0.5$. The remaining 29 sources have $L \lesssim 100$. Two of the four hard X-ray emitters in our sample (NX 13 and 32) were previously detected with *Einstein* and identified with galaxies (see Section 3.2.3 for details). They are the eighth and second brightest sources in this *XMM-Newton* field, respectively. The other two galaxies are NX 12 and 26 (with $L =$ 1601 and 394, respectively) and have no near-infrared counterpart (NX 26 has no optical counterpart, either).

The study of the X-ray properties of the AGNs in the field is far from the scope of this paper. Nevertheless, we show in Fig. A.4 the X-ray spectra observed here for NX 13 and NX 32, together with a simple fitting using a power-law, to compare with the spectra of the young stars (Figs. A.2 and A.3). The X-ray

[3] WebPIMMS is available at:
`http://heasarc.nasa.gov/Tools/w3pimms.html`.

spectra of these sources are clearly distinguishable from those of the young stars in our sample.

5. Summary and final remarks

We used archived data from the *XMM-Newton* mission to explore a region to the west of the centre of the σ Orionis cluster, slightly overlapped with a previous observation centred on the eponymous stellar system σ Ori. Our aim was to search for new X-ray young stars in the region and determine their X-ray properties. After a careful inspection of the source list resultant from the use of a maximum likelihood technique to reveal sources in the images of the EPIC cameras, we kept 41 X-ray sources. Among them, a total of 15 are young stars, 4 are field stars, and 19 are AGNs. The remaining three sources are of unknown nature, probably AGNs given their hardness ratios. Many of the revealed X-ray sources, including those associated to young stars, are new.

We derived X-ray parameters of the twelve young stars with enough counts for a spectral fitting, using multi-temperature models with absorption. In particular, we determined the column density, temperature of the thermal components, and metallicities. We observed no relation among the stars showing infrared excess and the column density measured here. Although we could not perform a detailed study of the X-ray variability because of the high variable background affecting the observation, two clear flaring events in the M-type young stars NX 17 (Mayrit 1298302) and NX 27 (Mayrit 797272) were studied. In both cases, we determined high coronal temperatures, reaching 38 and 50 MK, respectively. We also determined upper limits for the X-ray flux of young stars and brown dwarfs in the field that were not detected by the searching algorithm used by us.

Deep X-ray observations, combined with photometric data, have historically revealed as a powerful tool for disclosing the stellar population of star-forming regions down to the substellar boundary. In particular, in σ Orionis we were able to detect X-ray emission of mid-M type stars. Our work complements previous investigations on the X-ray population of this cluster. Our study also advances in the knowledge of the X-ray properties of young stars in the external region of the cluster, where the stellar density drops. Deeper X-ray observations in this region should permit to detect also the X-ray counterparts of brown dwarfs (as it was done in the cluster centre). The combination of their X-ray properties with the results of near- and mid-infrared photometry (to reveal the presence of discs) will permit to unveil the origin of the X-ray emission of these objects (whether it is produced by accretion or by a hot corona, as in pre-main sequence stars). This work should be followed by the study of the frequency of brown dwarfs with and without disc showing X-ray emission. A detailed study on the X-ray luminosity function of σ Orionis, compared with other young stellar clusters, will be addressed in a forthcoming paper by the authors.

Acknowledgements. We thank the anonymous referee for helpful comments. J.L.S. is an AstroCAM post-doctoral fellow at the UCM. J.A.C. is an Investigador Juan de la Cierva at the UCM. Partial financial support was provided by the Universidad Complutense de Madrid and the Spanish Ministerio Educación y Ciencia and the European Social Fund under grant AYA2005–02750 of the Programa Nacional de Astronomía y Astrofísica and by the Comunidad Autónoma de Madrid under PRICIT project S–0505/ESP–0237 (AstroCAM). J.L.S. also acknowledges financial contribution by the Marie Curie Actions grant No. MERG-CT-2007-046535.

References

Adams, N. R., Wolk, S. J., Walter, F. M., & Sherry, W. H. 2004, American Astronomical Society Meeting 205, #105.08
Alcalá, J. M., Terranegra, L., Wichmann, R., et al. 1996, A&AS, 119, 7
Alexander, D. M., Bauer, F. E., Brandt, W. N., et al. 2003, AJ, 125, 383
Anders, E., & Grevesse, N. 1989, Geochimica et Cosmochimica Acta 53, 197
Arnaud, K. 1996, XSPEC: The First Ten Years. In ASP Conf. Ser. 101, eds. G. H. Jacoby & J. Barnes, 17
Arnaud, K. 2004, XSPEC: Progress and Plans. In the American Astronomical Society, HEAD meeting 8, 16.29
Barrado y Navascués, D., Zapatero Osorio, M. R., Béjar, V. J. S., et al. 2001, A&A, 377, L9
Barrado y Navascués, D., Béjar, V. J. S., Mundt, R., et al. 2003, A&A, 404, 171
Béjar, V. J. S., Zapatero Osorio, M. R. & Rebolo, R. 1999, ApJ, 521, 671
Béjar, V. J. S., Martín, E. L., Zapatero Osorio, M. R., et al. 2001, ApJ, 556, 830
Béjar, V. J. S., Zapatero Osorio, M. R., & Rebolo, R. 2004, AN, 325, 705
Berghöfer, T. W., & Schmitt, J. H. M. M. 1994, A&A, 292, L5
Bonnarel, F., Fernique, P., Bienaymé, O., et al. 2000, A&AS, 143, 33
Bouy, H. 2004, A&A, 424, 619
Bouy, H., Huélamo, N., Martín, E. L., et al. 2008, A&A, in press (eprint arXiv:0808.3890)
Briggs, K. R., & Pye, J. P, 2004, MNRAS, 353, 673
Caballero, J. A. 2006, PhD thesis, Universidad de la Laguna, Spain
Caballero, J. A. 2007a, A&A, 466, 917
Caballero, J. A. 2007b, AN, 328, 917
Caballero, J. A. 2008a, MNRAS, 383, 375
Caballero, J. A. 2008b, MNRAS, 383, 750
Caballero, J. A. 2008c, A&A, 478, 667
Caballero, J. A., & Solano, E. 2008, A&A, 485, 931
Caballero, J. A., Béjar, V. J. S., Rebolo, R., Zapatero Osorio, M. R. 2004, A&A, 424, 857
Caballero, J. A., Martín, E. L., Dobbie, P. D., Barrado y Navascués, D. 2006, A&A, 460, 635
Caballero, J. A., Béjar, V. J. S., Rebolo, R. et al. 2007, A&A, 470, 903
Caballero, J. A., Valdivieso, L., Martín, E. L., et al. 2008, A&A, accepted
Chen, B., Stoughton, C., Smith, J. A., et al. 2001, ApJ, 553, 184
Chlebowski, T., Harnden, F. R., Jr., & Sciortino, S. 1989, ApJ, 341, 427
Comastri, A., Setti, G., Zamorani, G., & Hasinger, G. 1995, A&A, 296, 1
Crespo-Chacón, I., Micela, G., Reale, F., et al. 2007, A&A, 471, 929
Della Ceca, R., Maccacaro, T., Caccianiga, A., et al. 2004, A&A, 428, 383
Epchtein, N., de Batz, B., Capoani, L., et al. 1997, Msngr, 87, 27
Favata, F., Flaccomio, E., Reale, F., et al. 2005, ApJS, 160, 469
Feigelson, E. D., Getman, K., Townsley, L., et al. 2005, ApJS, 160, 379
Franciosini, E., Pallavicini, R., & Sanz-Forcada, J. 2006, A&A, 446, 501
Franciosini, E., Pillitteri, I., Stelzer, B., et al. 2007, A&A, 468, 485
Garrison, R. F. 1967, PASP, 79, 433
González-Hernández, J. I., Caballero, J. A., Rebolo, R., et al. 2008, A&A, in press (eprint arXiv:0809.0090)
Groote, D., & Hunger, K., 1982, A&A, 116, 64
Groote, D., & Schmitt, J. H. M. M. 2004, A&A, 418, 235
Habing, H. J., Tignon, J., & Tielens, A. G. G. M. 1994, A&A, 286, 523
Hernández, J., Calvet, N., Hartmann, L., et al. 2005, AJ, 129, 856
Hernández, J., Hartmann, L., Megeath, T. et al. 2007, ApJ, 662, 1067
Høg, E., Fabricius, C., Makarov, V. V., et al. 2000, A&A, 355, L27
Imanishi, K., Tsujimoto, M., & Koyama, K. 2001, ApJ, 563, 361
Jeffries, R. D., Maxted, P. F. L., Oliveira, J. M., & Naylor, T. 2006, MNRAS, 371, L6
Kenyon, M. J., Jeffries, R. D., Naylor, T., Oliveira, J. M., & Maxted, P. F. L. 2005, MNRAS, 356, 89
Landstreet, J. D., & Borra, E. F. 1978, ApJ, 224, L5
Lee, T. A. 1968, ApJ, 152, 913
Lee, C. W., Martín, E. L., & Mathieu, R. D. 1994, AJ, 108, 1445
Luhman, K. L., Hernández, J., Downes, J. J., Hartmann, L., & Briceño, C. 2008, ApJ, in press (eprint arXiv:0808.0471)
Maxted, P. F. L., Jeffries, R. D., Oliveira, J. M., Naylor, T., & Jackson, R. J. 2008, MNRAS, 385, 2210
Mohanty, S., & Basri, G. 2003, ApJ, 583, 451
Mokler, F., & Stelzer, B. 2002, A&A, 391, 1025
Monet, D. G., Levine, S. E., Canzian, B., et al. 2003, AJ, 125, 984
Morrison, R., & McCammon, D. 1983, ApJ, 270, 119
Muzerolle, J., Hillenbrand, L., Calvet, N., Briceño, C., & Hartmann, L. 2003, ApJ, 592, 266
Nakano, M., Yamauchi, S., Sugitani, K., Ogura, K., & Kogure, T. 1999, PASJ, 51, 1
Neuhäuser, R., & Comerón, F. 1998, Science, 282, 83
Neuhäuser, R., Sterzik, M. F., Schmitt, J. H. M. M., Wichmann, R., & Krautter, J. 1995, A&A, 297, 391

Neuhäuser, R., Briceño, C., Comerón, F., et al. 1999, A&A, 343, 883
Preibisch, T., McCaughrean, M. J., Grosso, N., et al. 2005, ApJS, 160, 582
Rees, M. J. 1984, ARA&A, 22, 471
Reipurth, B., Devine, D., & Bally, J. 1998, AJ, 116, 1396
Robrade, J., & Schmitt, J. H. M. M 2005, A&A, 435, 1073
Rutledge, R. E., Basri, G., Martín, E. L., & Bildsten, L. 2000, ApJ, 538, L141
Sanz-Forcada, J., Franciosini, E., Pallavicini, R. 2004, A&A, 421, 715
Scholz, A., & Eislöffel, J. 2004, A&A, 421, 259
Scholz, A., & Jayawardhana, R. 2008, ApJ, 672, L49
Sherry, W. H., Walter, F. M., & Wolk, S. J. 2004, AJ, 128, 2316
Sherry, W. H., Walter, F. M., Wolk, S. J., & Adams, N. R. 2008, AJ, 135, 1616
Skinner, S. L., Sokal, K. R., Cohen, D. H., et al. 2008, ApJ, 683, 796
Skrutskie, M. F., Cutri, R. M., Stiening, R., et al. 2006, AJ, 131, 1163
Smith, R. K., Brickhouse, N. S., Liedahl, D. A., & Raymond, J. C. 2001, ApJ, 556, L91
Stelzer, B. 2004, ApJ, 615, L153
Stocke, J. T., Morris, S. L., Gioia, I. M., et al. 1991, ApJS, 76, 813
Tsuboi, Y., Maeda, Y., Feigelson, E. D., et al. 2003, ApJ, 587, L51
Ueda, Y., Akiyama, M., Ohta, K., & Miyaji, T. 2003, ApJ, 598, 886
Walborn, N. R. 1974, ApJ, 191, L95
Waldron, W. L., & Cassinelli, J. P. 2007, ApJ, 668, 456
Walter, F. M., Wolk, S. J., Freyberg, M., & Schmitt, J. H. M. M. 1997, MmSAI, 68, 1081
Watson, M. G., Pye, J. P., Denby, M., et al. 2003, AN, 324, 89
Wiramihardja, S. D., Kogure, T., Yoshida, S., Ogura, K., Nakano, M. 1989, PASJ, 41, 155
Wiramihardja, S. D., Kogure, T., Yoshida, S., et al. 1991, PASJ, 43, 27
Wolk, S. J. 1996, PhD thesis, State University of New York at Stony Brook, USA
Zapatero Osorio, M. R., Béjar, V. J. S., Martín, E. L., et al. 2000, Science, 290, 103
Zapatero Osorio, M. R., Béjar, V. J. S., Martín, E. L., Barrado y Navascués, D., & Rebolo, R. 2002a, ApJ, 569, L99
Zapatero Osorio, M. R., Béjar, V. J. S., Martín, E. L., et al. 2002b, ApJ, 578, 536
Zapatero Osorio, M. R., Caballero, J. A., Béjar, V. J. S., et al. 2007, A&A, 472, L9
Zapatero Osorio, M. R., Béjar, V. J. S., Bihain, G., et al. 2008, A&A, 477, 895

Appendix A: On-line material

Table A.1. Detected X-ray sources in the combined images of the EPIC cameras.

NX	α	δ	L	CR [ks^{-1}]			HR_1	HR_2
	(J2000)	(J2000)		PN	MOS1	MOS2		
1	05 36 46.30	–02 35 04.0	27	9.8 ± 1.8	...	3.8 ± 0.7	–0.76 ± 0.20	+0.15 ± 0.20
2	05 36 50.88	–02 24 52.5	45	15.3 ± 2.2	4.8 ± 1.0	6.1 ± 0.9	–0.40 ± 0.13	–1.00 ± 0.13
3	05 36 56.28	–02 42 12.2	16	...	...	4.3 ± 0.9	+0.08 ± 0.21	–0.45 ± 0.21
4	05 37 10.25	–02 30 09.5	15	4.3 ± 1.0	...	...	–0.81 ± 0.21	+0.14 ± 0.21
5	05 37 11.46	–02 32 10.6	5375	114.0 ± 2.3	30.7 ± 1.0	31.3 ± 1.0	–0.94 ± 0.01	–1.00 ± 0.01
6	05 37 13.81	–02 43 54.2	18	8.6 ± 1.9	...	3.2 ± 0.7	–0.68 ± 0.22	–0.26 ± 0.22
7	05 37 15.20	–02 30 55.5	2235	61.1 ± 1.8	17.0 ± 0.8	19.6 ± 0.8	–0.89 ± 0.02	–0.90 ± 0.02
8	05 37 19.63	–02 25 41.7	24	6.7 ± 1.2	...	...	–0.51 ± 0.17	–1.00 ± 0.17
9	05 37 20.91	–02 37 20.4	21	3.7 ± 0.7	...	1.8 ± 0.4	–1.00 ± 0.07	...
10	05 37 22.75	–02 22 42.5	19	7.7 ± 1.5	...	3.2 ± 0.6	–0.34 ± 0.18	–0.49 ± 0.18
11	05 37 22.81	–02 32 47.2	27	...	1.7 ± 0.3	1.3 ± 0.3	–0.81 ± 0.19	–0.05 ± 0.19
12	05 37 23.95	–02 42 01.1	1601	88.1 ± 2.8	32.9 ± 1.3	32.8 ± 1.6	–0.54 ± 0.03	–0.26 ± 0.03
13	05 37 27.84	–02 40 04.0	2597	...	57.0 ± 1.8	49.5 ± 1.6	–0.59 ± 0.03	–0.70 ± 0.03
14	05 37 28.00	–02 36 09.1	91	7.1 ± 0.8	1.7 ± 0.3	...	–0.99 ± 0.06	–1.00 ± 0.06
15	05 37 28.29	–02 32 45.8	63	6.4 ± 0.8	1.7 ± 0.3	2.2 ± 0.3	–0.67 ± 0.12	–0.51 ± 0.12
16	05 37 28.36	–02 24 19.9	17	...	1.8 ± 0.4	...	–0.92 ± 0.18	–1.00 ± 0.18
17	05 37 31.30	–02 24 28.9	1422	61.2 ± 2.2	15.7 ± 1.0	16.1 ± 0.9	–0.81 ± 0.03	–0.60 ± 0.03
18	05 37 31.53	–02 25 12.0	58	8.7 ± 1.2	2.1 ± 0.5	1.9 ± 0.4	–0.62 ± 0.13	–0.58 ± 0.13
19	05 37 32.95	–02 37 45.6	35	5.8 ± 0.9	2.0 ± 0.4	2.3 ± 0.5	–0.47 ± 0.15	–0.70 ± 0.15
20	05 37 36.47	–02 34 02.7	122	10.0 ± 1.0	2.8 ± 0.4	3.3 ± 0.4	–0.87 ± 0.09	–1.00 ± 0.09
21	05 37 37.67	–02 45 45.1	102	18.1 ± 2.0	5.2 ± 0.8	6.2 ± 0.9	–0.84 ± 0.10	–1.00 ± 0.10
22	05 37 41.58	–02 29 10.8	43	5.0 ± 0.8	...	1.3 ± 0.3	–0.88 ± 0.14	–1.00 ± 0.14
23	05 37 41.84	–02 29 39.8	79	9.2 ± 1.0	2.9 ± 0.4	2.7 ± 0.4	–0.42 ± 0.11	–0.62 ± 0.11
24	05 37 42.71	–02 25 13.5	23	19.8 ± 3.8	2.5 ± 0.5	3.1 ± 0.5	–0.79 ± 0.21	+0.37 ± 0.21
25	05 37 43.38	–02 27 53.6	21	...	...	2.2 ± 0.4	+0.07 ± 0.19	–0.40 ± 0.19
26	05 37 47.56	–02 29 10.2	394	24.4 ± 1.3	9.1 ± 0.6	9.3 ± 0.6	–0.27 ± 0.05	–0.45 ± 0.05
27	05 37 51.45	–02 35 26.2	6907	136.8 ± 2.5	39.2 ± 1.4	40.6 ± 1.1	–0.82 ± 0.01	–0.58 ± 0.01
28	05 37 52.83	–02 33 34.9	2643	322.5 ± 8.2	98.0 ± 1.7	...	–0.85 ± 0.02	–0.61 ± 0.02
29	05 37 53.27	–02 26 54.7	21	13.0 ± 2.5	2.6 ± 0.6	...	–0.70 ± 0.20	+0.26 ± 0.20
30	05 37 54.25	–02 39 30.8	32606	547.1 ± 5.3	153.8 ± 2.4	157.6 ± 2.5	–0.85 ± 0.01	–0.70 ± 0.01
31	05 37 55.74	–02 33 43.0	17	...	4.1 ± 0.8	...	–0.90 ± 0.16	–1.00 ± 0.16
32	05 37 56.20	–02 45 13.8	26045	883.0 ± 8.9	...	282.3 ± 4.3	–0.60 ± 0.01	–0.40 ± 0.01
33	05 37 58.07	–02 25 14.0	34	8.8 ± 1.4	3.2 ± 0.6	4.0 ± 0.6	–0.42 ± 0.15	–0.42 ± 0.15
34	05 38 01.43	–02 25 54.2	95	12.1 ± 1.4	4.6 ± 0.6	4.1 ± 0.6	–0.84 ± 0.10	–1.00 ± 0.10
35	05 38 03.68	–02 27 30.0	16	4.8 ± 1.0	...	...	–0.65 ± 0.22	–1.00 ± 0.22
36	05 38 06.57	–02 30 23.9	24	5.3 ± 1.0	2.3 ± 0.5	...	–0.82 ± 0.18	–0.85 ± 0.18
37	05 38 07.65	–02 31 32.3	8021	205.0 ± 3.7	62.9 ± 1.9	57.9 ± 1.5	–0.89 ± 0.01	–0.80 ± 0.01
38	05 38 08.06	–02 35 57.3	749	38.7 ± 1.8	11.4 ± 0.8	10.6 ± 0.8	–0.85 ± 0.04	–0.52 ± 0.04
39	05 38 13.60	–02 35 09.7	143	16.3 ± 1.5	5.7 ± 0.7	4.8 ± 0.7	–0.67 ± 0.08	–0.81 ± 0.08
40	05 38 14.02	–02 36 48.3	15	...	2.8 ± 0.6	4.6 ± 0.7	–0.06 ± 0.22	–0.34 ± 0.22
41	05 38 15.42	–02 42 11.7	30	12.4 ± 2.1	5.4 ± 1.0	...	–0.47 ± 0.16	–0.48 ± 0.16

Table A.2. USNO-B1/DENIS/2MASS counterparts of the X-ray sources in Table A.1.

NX	α (J2000)	δ (J2000)	B_J [mag]	i [mag]	$J \pm \delta J$ [mag]	$H \pm \delta H$ [mag]	$K_s \pm \delta K_s$ [mag]	Alternative name
1	...	...	$\gtrsim$21	$\gtrsim$18.0	$\gtrsim$17.1	$\gtrsim$16.4	$\gtrsim$14.3	...
2	...	...	$\gtrsim$21	$\gtrsim$18.0	$\gtrsim$17.1	$\gtrsim$16.4	$\gtrsim$14.3	...
3	05 36 56.29	–02 42 07.4	19.9	18.6	$\gtrsim$17.1	$\gtrsim$16.4	$\gtrsim$14.3	USNO–B1.0 0872–0105742
4	05 37 10.47	–02 30 07.2	12.23±0.16	11.31	10.72±0.05	10.46±0.05	10.30±0.04	TYC 4770–1261–1
5	05 37 11.61	–02 32 08.8	13.6	11.65	10.88±0.02	10.29±0.02	10.07±0.02	OriNTT 429 AB
6	05 37 13.92	–02 43 51.7	16.2	14.32	13.50±0.03	12.81±0.03	12.74±0.03	2MASS J05371392–0243517
7	05 37 15.37	–02 30 53.4	13.5	12.18	11.36±0.02	11.01±0.02	10.88±0.02	SO211394
8	...	...	$\gtrsim$21	$\gtrsim$18.0	$\gtrsim$17.1	$\gtrsim$16.4	$\gtrsim$14.3	...
9	05 37 21.07	–02 37 19.2	15.9	14.25	13.27±0.03	12.76±0.03	12.60±0.03	2MASS J05372107–0237192
10	05 37 23.05	–02 22 43.1	16.9	16.28	15.46±0.06	15.07±0.10	14.88±0.14	2MASS J05372304–0222431
11	05 37 22.78	–02 32 42.9	16.6	15.26	14.36±0.04	13.84±0.04	13.82±0.06	2MASS J05372277–0232429
	05 37 23.06	–02 32 46.6	19.0	15.78	14.18±0.04	13.59±0.04	13.41±0.05	2MASS J05372306–0232465
12	05 37 24.11	–02 41 59.9	18.9	18.41	$\gtrsim$17.1	$\gtrsim$16.4	$\gtrsim$14.3	DENIS J05372411–0241599
13	05 37 27.94	–02 40 03.2	15.8	16.19	14.82±0.08	14.09±0.07	14.43±0.07	2E 1448
14	05 37 28.07	–02 36 06.6	18.5	15.27	13.74±0.03	13.08±0.03	12.80±0.03	2MASS J05372806–0236065
15	...	...	$\gtrsim$21	$\gtrsim$18.0	$\gtrsim$17.1	$\gtrsim$16.4	$\gtrsim$14.3	...
16	05 37 28.32	–02 24 18.2	18.6	15.61	14.00±0.03	13.39±0.03	13.08±0.03	2MASS J05372831–0224182
17	05 37 31.54	–02 24 27.0	16.5	13.63	12.11±0.03	11.36±0.02	11.17±0.02	[SWW2004] 137
18	05 37 31.68	–02 25 10.6	19.7	18.8	$\gtrsim$17.1	$\gtrsim$16.4	$\gtrsim$14.3	USNO–B1.0 0875–0102588
19	05 37 32.97	–02 37 44.2	20.7	$\gtrsim$18.0	$\gtrsim$17.1	$\gtrsim$16.4	$\gtrsim$14.3	USNO–B1.0 0873–0105537
20	05 37 36.67	–02 34 00.3	17.5	14.56	13.00±0.03	12.30±0.02	12.05±0.02	[SWW2004] 141
21	05 37 37.84	–02 45 44.2	17.5	14.17	12.69±0.03	11.94±0.02	11.72±0.03	2MASS J05373784–0245442
22	05 37 41.79	–02 29 08.1	11.23±0.06	10.39	9.80±0.03	9.60±0.03	9.50±0.03	TYC 4771–621–1
23	05 37 41.61	–02 29 38.0	16.5	14.85	13.70±0.03	13.11±0.02	12.94±0.03	2MASS J05374160–0229380
24	05 37 43.10	–02 25 13.1	15.1	13.46	12.54±0.03	12.03±0.02	11.97±0.03	2MASS J05374310–0225131
25	...	...	$\gtrsim$21	$\gtrsim$18.0	$\gtrsim$17.1	$\gtrsim$16.4	$\gtrsim$14.3	...
26	...	...	$\gtrsim$21	$\gtrsim$18.0	$\gtrsim$17.1	$\gtrsim$16.4	$\gtrsim$14.3	...
27	05 37 51.61	–02 35 25.7	16.6	13.45	11.89±0.03	11.17±0.02	10.98±0.02	[SWW2004] 125
28	05 37 53.03	–02 33 34.4	12.4	10.80	9.99±0.03	9.60±0.02	9.47±0.02	2E 1454
29	...	...	$\gtrsim$21	$\gtrsim$18.0	$\gtrsim$17.1	$\gtrsim$16.4	$\gtrsim$14.3	...
30	05 37 54.40	–02 39 29.8	12.02±0.12	10.27	9.26±0.02	8.72±0.05	8.61±0.02	2E 1455
31	...	...	$\gtrsim$21	$\gtrsim$18.0	$\gtrsim$17.1	$\gtrsim$16.4	$\gtrsim$14.3	...
32	05 37 56.31	–02 45 13.1	16.4	16.73	15.40±0.07	14.52±0.08	13.72±0.07	2E 1456
33	05 37 58.36	–02 25 13.1	19.7	$\gtrsim$18.0	$\gtrsim$17.1	$\gtrsim$16.4	$\gtrsim$14.3	USNO–B1.0 0875–0102882
34	05 38 01.67	–02 25 52.7	17.5	14.65	13.03±0.03	12.32±0.02	12.07±0.03	[SE2004] 53
35	...	...	$\gtrsim$21	$\gtrsim$18.0	$\gtrsim$17.1	$\gtrsim$16.4	$\gtrsim$14.3	...
36	05 38 06.74	–02 30 22.8	15.8	13.23	11.76±0.03	10.92±0.02	10.54±0.02	Kiso A–0904 67
37	05 38 07.85	–02 31 31.4	13.3	11.63	10.57±0.03	9.93±0.02	9.77±0.02	2E 1459
38	05 38 08.27	–02 35 56.3	16.3	13.97	12.14±0.03	11.38±0.02	11.047±0.019	Kiso A–0976 316
39	...	...	$\gtrsim$21	$\gtrsim$18.0	$\gtrsim$17.1	$\gtrsim$16.4	$\gtrsim$14.3	...
40	...	...	$\gtrsim$21	$\gtrsim$18.0	$\gtrsim$17.1	$\gtrsim$16.4	$\gtrsim$14.3	...
41	05 38 15.53	–02 42 05.1	18.0	17.25	16.33±0.09	15.61±0.09	15.5:	2MASS J05381552–0242051

Table A.3. Upper limits (3σ) for undetected σ Orionis cluster members and candidates in the *XMM-Newton* field.

Mayrit	Alternative name	α (J2000)	δ (J2000)	Youth features	F_X^a [10^{-13} erg cm^{-2} s^{-1}]	Remarks
1773275	[SWW2004] 13	05 36 46.91	–02 33 28.3	Li I, low *g*	...	In PN gap
1599271	S Ori 33	05 36 58.08	–02 35 19.4	...	<0.29	...
1630286	[SWW2004] 90	05 37 00.30	–02 28 26.6	...	<0.33	...
1738301	...	05 37 05.17	–02 21 09.4	...	...	In MOS border. Out of PN field
1416280	[SWW2004] 22	05 37 11.68	–02 31 56.7	...	...	Blended with NX 5
1391255	S Ori J053715.1–024202	05 37 15.16	–02 42 01.6	Li I, Hα	<0.27	...
1225282	S Ori 66	05 37 24.70	–02 31 52.0	Hα, II?	<0.26	...
1185274	S Ori 55	05 37 25.90	–02 34 32.0	Hα, II?	<0.22	...
1329304	Haro 5–5	05 37 30.95	–02 23 42.8	Hα, II	<0.29	Marginally detected
1227243	HD 294275	05 37 31.87	–02 45 18.5	OB	...	In PN gap
1176297	[HHM2007] 107	05 37 35.14	–02 26 57.7	...	<0.23	...
1116300	HD 37333	05 37 40.48	–02 26 36.8	OB, Si II	<0.19	...
968292	GSC 04771–00962	05 37 44.92	–02 29 57.3	...	<0.22	...
958292	SO210868	05 37 45.57	–02 29 58.5	Li I	...	In PN gap
999306	S Ori 23	05 37 51.11	–02 26 07.5	...	<0.25	...
790270	[KJN2005] 62	05 37 52.07	–02 36 04.7	Li I, low *g*	<0.26	Marginally detected
882239	...	05 37 54.45	–02 43 37.8	...	<0.33	...
809248	[SWW2004] 174	05 37 54.86	–02 41 09.2	Li I, low *g*	<0.37	Marginally detected
757283	S Ori 35	05 37 55.60	–02 33 05.3	II	<0.23	...
728257	S Ori 12	05 37 57.46	–02 38 44.4	Li I, Hα, low *g*, II	<0.26	...
767245	[OJV2004] 28	05 37 58.40	–02 41 26.2	Li I, low *g*	<0.28	...
861230	[SWW2004] 140	05 38 00.56	–02 45 09.7	...	...	[FPS2006] 4. Close to PN border and to NX 32
884312	[WB2004] 13	05 38 00.97	–02 26 07.9	trans. disc, Hα?	<0.27	...
873229	Haro 5–7	05 38 01.07	–02 45 38.0	Hα, II	<0.41	...
588270	S Ori J053805.5–023557	05 38 05.52	–02 35 57.1	II	<0.20	...
717307	[W96] 4771–0950	05 38 06.50	–02 28 49.4	Li I	...	[FPS2006] 6. In PN gap
520267	S Ori 70	05 38 10.10	–02 36 26.0	low *g*?	<0.34	...
757321	[SWW2004] 233	05 38 13.20	–02 26 08.8	Li I, Hα, II	...	[FPS2006] 11. In PN border
447254	S Ori J053816.0–023805	05 38 16.10	–02 38 04.9	Li I, low *g*	<0.29	...
488237	S Ori 27	05 38 17.42	–02 40 24.3	Li I, Hα, low *g*	<0.27	...
498234	S Ori J053817.8–024050	05 38 17.78	–02 40 50.1	II	...	[FPS2006] 17. In PN border. Marginally detected in MOS2
396273	S Ori J053818.2–023539	05 38 18.35	–02 35 38.6	low *g*	<0.29	[FPS2006] 19
387252	S Ori J053820.1–023802	05 38 20.21	–02 38 01.6	Li I, Hα, II	<0.34	[FPS2006] 20. Close to PN border. Marginally detected
380287	[W96] r053820–0234	05 38 20.50	–02 34 09.0	Li I, Hα	...	...
379292	S Ori J053821.3–023336	05 38 21.38	–02 33 36.3	Li I, low *g*	...	...
329261	[SWW2004] 207	05 38 23.08	–02 36 49.4	low *g*, II	...	...
399314	S Ori 18	05 38 25.68	–02 31 21.7	Li I, low *g*	...	In MOS gap. Out of PN field
265282	Kiso A–0976 329	05 38 27.51	–02 35 04.2	Li I, Hα, II	...	[FPS2006] 33. In MOS border. Out of PN field

[a] For each star/brown dwarf, the flux upper limit was calculated from its count-rate using a Raymond Smith model with $T = 1$ keV and $N_{\rm H} = 0.27 \times 10^{21}$ cm^{-2}. To determine the count-rate, we used a 15 arcsec extraction radius in the position of the Mayrit source.

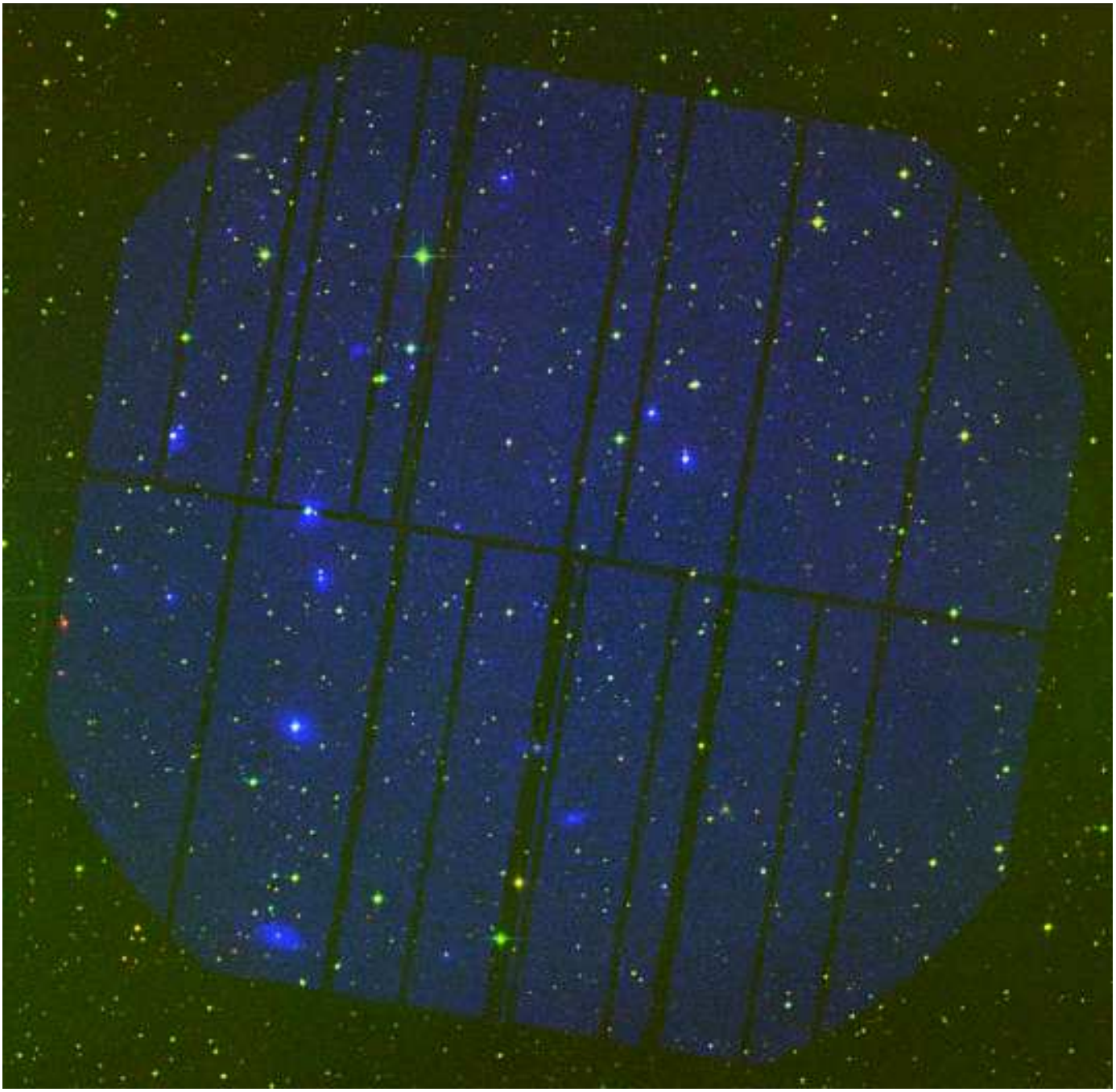

Fig. A.1. False colour image combining 2MASS K_s (red), photographic R_F DSS2 Red (green), and our *XMM-Newton* EPIC+MOS1+MOS2 (blue) data. The field of view of *XMM-Newton* (approximate 30×30 arcmin^2) is clearly discernible. North is up and east is left.

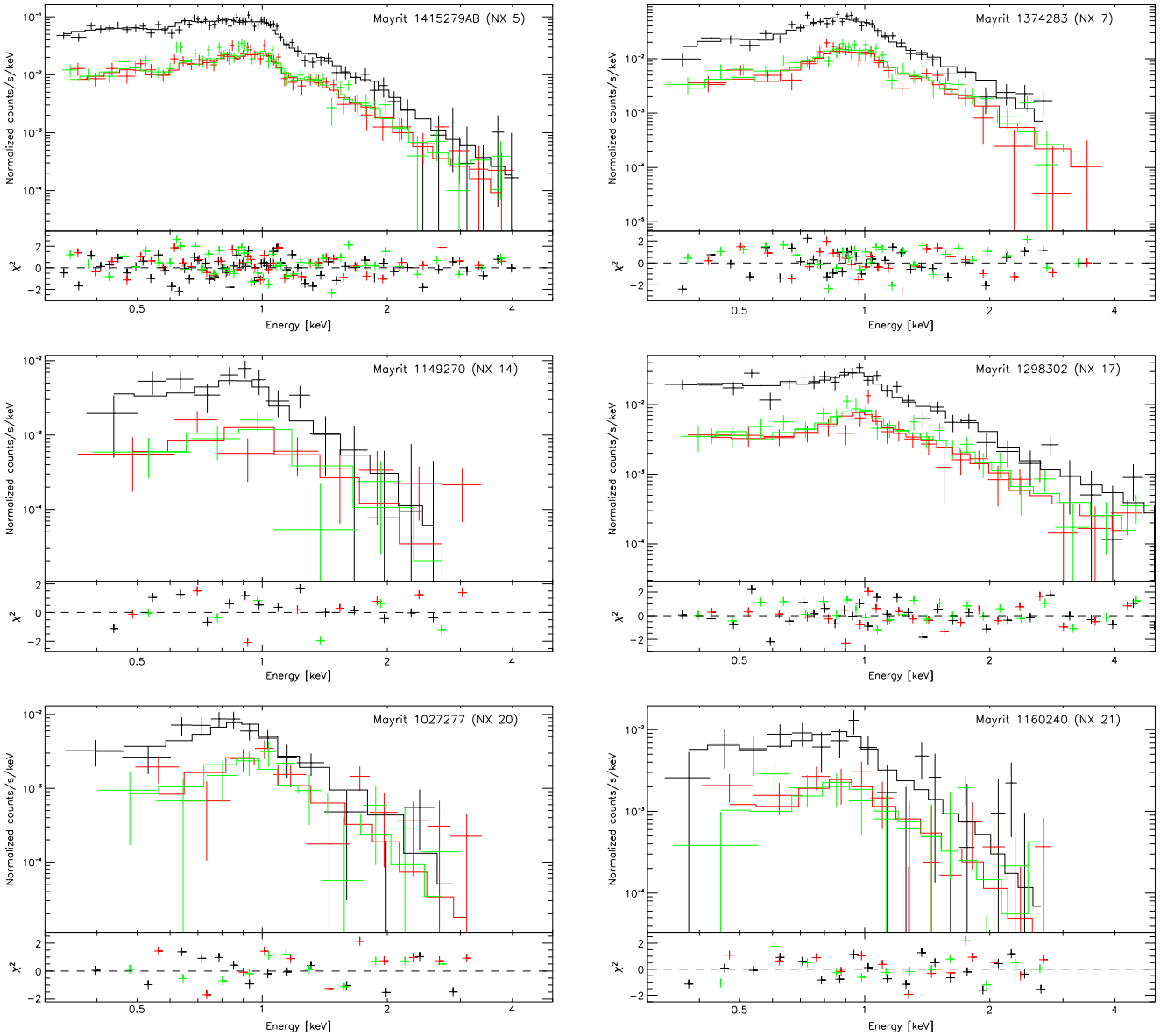

Fig. A.2. Spectral energy distributions of six young stars and candidates in the σ Orionis cluster. Each name is labelled. The spectra were binned so that each bin contains a minimum of 10 counts. Different line styles correspond to the PN [black], MOS1 [red], and MOS2 [green] cameras and their corresponding spectral fittings (see Table 3). The bottom part of each panel illustrates the quality of the fitting.

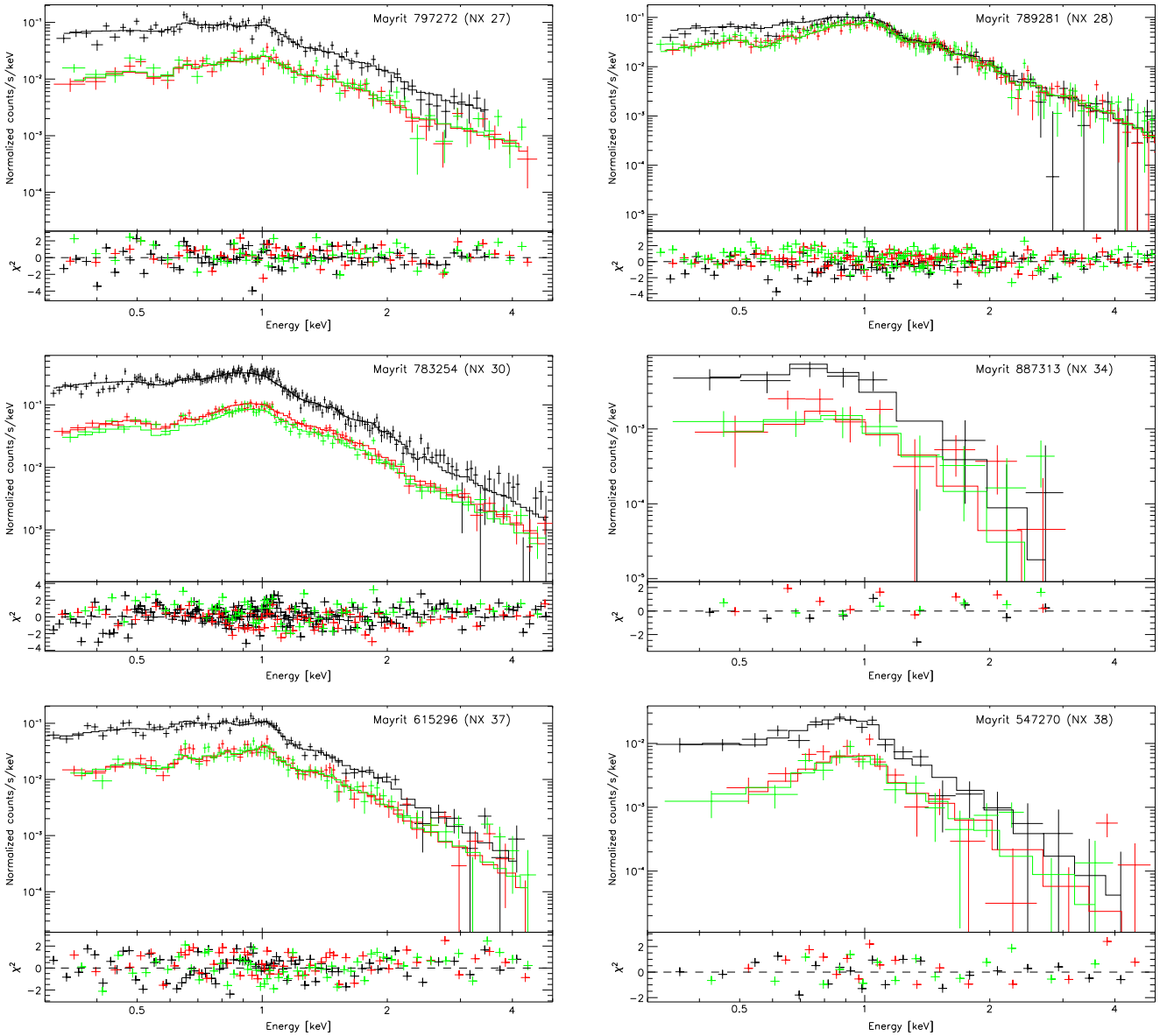

Fig. A.3. Same as Fig. A.2, but for the remaining six young stars and candidates in the σ Orionis cluster. The panel corresponding to NX 27 (top left) is for the 3T fitting (see Table 3).

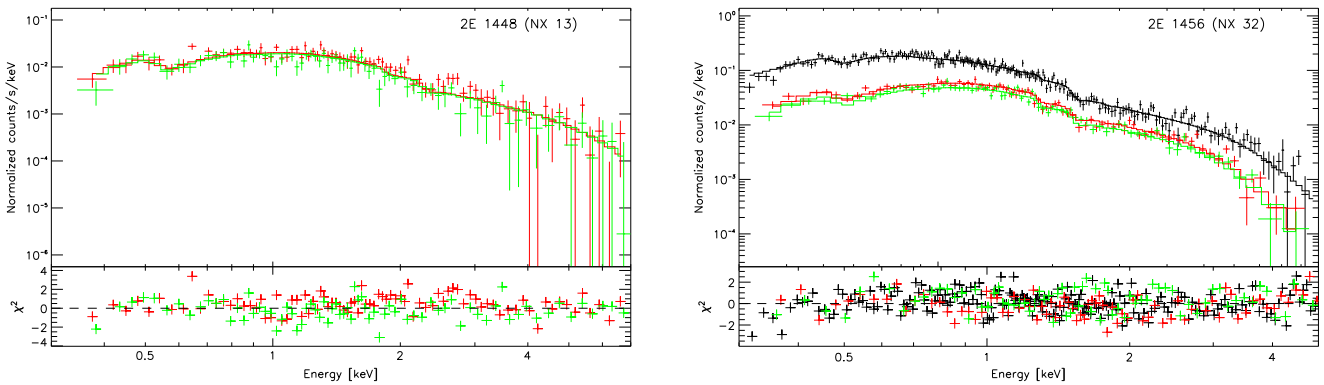

Fig. A.4. Same as Fig. A.2, but for two AGNs in the field: NX 13 and NX 32. The fittings were made using a power-law with parameters $N_{\rm H} = 2.05 \times 10^{21}$ cm^{-2}, photon power-law index $\Gamma = 2.43$ for NX 13; and $N_{\rm H} = 1.33 \times 10^{21}$ cm^{-2}, photon power law index $\Gamma = 1.82$ for NX 32.

List of Objects

‘σ Orionis’ on page 1
‘S Ori 70’ on page 1
‘σ Ori A’ on page 1
‘σ Ori E’ on page 1
‘GD 257’ on page 2
‘Mayrit 633059’ on page 2
‘Mayrit 433123’ on page 2
‘Mayrit 487350’ on page 2
‘Mayrit 396273’ on page 2
‘S Ori 55’ on page 2
‘S Ori 66’ on page 9
‘LP 944–20’ on page 10
‘GJ 569B’ on page 10
‘TYC 4770–1261–1’ on page 14
‘OriNTT 429’ on page 14
‘SO211394’ on page 14
‘2E 1448’ on page 14
‘[SWW2004] 137’ on page 14
‘[SWW2004] 141’ on page 14
‘TYC 4771–621–1’ on page 14
‘[SWW2004] 125’ on page 14
‘2E 1454’ on page 14
‘2E 1455’ on page 14
‘2E 1456’ on page 14
‘[SE2004] 53’ on page 14
‘Kiso A–0904 67’ on page 14
‘2E 1459’ on page 14
‘Kiso A–0976 316’ on page 14
‘2MASS J05381552–0242051’ on page 14